COLLOIDAL PLEXCITONIC NANOCRYSTALS

**A Thesis Submitted to
the Graduate School of
İzmir Institute of Technology
in Partial Fulfillment of the Requirements for the Degree of**

MASTER OF SCIENCE

in Chemistry

**by
Sema SARISÖZEN**

**June 2022
İZMİR**

ACKNOWLEDGEMENTS

always encouraging me to achieve everything I wanted, for always supporting me to go after my goals, for always having my back, for loving me, for lifting me up when I am down, for always making me smile, and for being my shoulder to cry on. I love you to the moon and back!

ABSTRACT

COLLOIDAL PLEXCITONIC NANOCRYSTALS

Noble metal nanocrystals, especially gold and silver, which have attracted a great deal of attention due to the supporting of surface plasmon polaritons (SPPs), have been extensively investigated and studied. With recent developments in colloid chemistry, synthesis of noble metal nanocrystals with tunable optical properties in the visible region of the electromagnetic spectrum has become easier. Until now, noble metal nanocrystals (NPs) synthesized by using various synthetic methods, have a variety of shapes, such as bipyramid, rod, disk, prism, and ring, etc. In the strong coupling regime, SPPs supported by metal nanocrystals interact strongly with excitons of organic dyes, semiconducting quantum dots (carbon or perovskite quantum dots) to generate a new hybrid optical mode called plexciton (plasmon-exciton). Plexcitonic nanocrystals have received interest owing to their ease of synthesis, scalability, and ability to provide sub-wavelength confinement of incident light and offer promising applications. Plasmon–exciton interaction at nanoscale dimension can be improved by generating new plexcitonic nanoparticles with tunable optical properties, which may be utilized in critical applications such as nanolasers, sensors, nano-optics, solar cells, and light emitting diodes. Therefore, there has been a tremendous amount of interest in the synthesis of new plexcitonic nanocrystals having excellent optical and chemical properties. The main goal of this thesis is to synthesize new plexcitonic nanoparticles with tunable optical properties in the visible spectrum: (i) synthesis of different shaped colloidal monometallic and bimetallic nanocrystals, (ii) synthesis of new colloidal plexcitonic nanocrystals, (iii) synthesis of carbon quantum dots (CDs), (iv) coupling of excitons of CDs and SPPs on the silver thin film.

ÖZET

KOLLOID PLEKZİTONİK NANOKRİSTALLER

Soy metal nanokristaller, özellikle altın ve gümüş, yüzey plazmon polaritonları desteklemeleri nedeniyle büyük ilgi görmüş, kapsamlı bir şekilde araştırılıp ve çalışılmıştır. Kolloid kimyasındaki son gelişmeler ile elektromanyetik spektrumun görünür bölgesinde ayarlanabilir optik özelliklere sahip asil metal nanokristallerin sentezi kolaylaşmıştır. Şimdiye kadar çeşitli sentetik yöntemler kullanılarak sentezlenen asil metal nanokristaller bipiramid, çubuk, disk, prizma ve halka vb. gibi çeşitli şekillere sahiptir. Güçlü birleştirme rejiminde, metal nanokristaller tarafından desteklenen yüzey plazmon polaritonları, plekziton (plazmon-eksiton) adı verilen yeni bir hibrit optik mod oluşturmak için organik boyaların, yarı iletken kuantum noktaların, karbon noktaların veya perovskitlerin eksitonları ile güçlü bir şekilde etkileşime girer. Plekzitonik nanokristaller, sentez kolaylıkları, ölçeklenebilirlikleri ve gelen ışığın sınırlandırılmasını sağlama yetenekleri ve umut verici uygulamalar sunmaları nedeniyle ilgi görmüştür. Nano boyuttaki plazmon-eksiton etkileşimi, nanolazerlerde, sensörlerde, nano-optiklerde, güneş pillerinde ve ışık yayan diyotlarda kritik uygulamalarda kullanılabilen ayarlanabilir optik özelliklere sahip yeni pleksitonik nanoparçacıklar üretilerek geliştirilebilir. Bu nedenle, mükemmel optik ve kimyasal özelliklere sahip yeni pleksitonik nanokristallerin sentezine büyük bir ilgi vardır. Bu tezin temel amacı, görünür spektrumda ayarlanabilir optik özelliklere sahip yeni pleksitonik nanopartiküllerin sentezlenmesidir: (i) farklı şekillere sahip kolloidal monometalik ve bimetalik nanokristallerin sentezi, (ii) yeni kolloidal pleksitonik nanokristallerin sentezi, (iii) karbon kuantum nokta sentezi, (iv) karbon kuantum noktaların eksitonları ve gümüş ince film tarafından desteklenen yüzey plasmon polaritonlarının etkileşimi.

TABLE OF CONTENTS

LIST OF FIGURES

CHAPTER 1

INTRODUCTION

When surface plasmon polaritons (SPPs) supported by metal nanoparticles interact strongly with molecular excitons or excitons of organic dyes, semiconducting quantum dots, and perovskites, hybrid particles showing half-plasmonic and half-excitonic characters are generated. The main goal of this thesis is to investigate strong interaction between SPPs generated by metal nanoparticles or metal thin films, and excitons of semiconductor organic dye or carbon dots. This part of the thesis involves general information about nanoparticles, plasmons, excitons, plexcitons, and liquid crystals.

1.1. Nanoparticles

Nanotechnology and nanoscience were introduced for the first time on December 29[th]1959 by Nobel laureate and a renowned physicist Richard P. Feynman at the famous conference "There's Plenty of Room at the Bottom"[14] and nobody knew that scientists would produce materials at the atomic and molecular level and make cutting-edge scientific discoveries by using them at those times. As time progressed, the ability to synthesize, characterize, manipulate, and control materials at nanoscale dimensions have gradually increased. Up until recently, many types of nanomaterials have been fabricated and synthesized at nanoscale dimension owing to the advancements in nanofabrication and colloid chemistry.

Nanoparticles are tiny particles of various shapes whose size is 1-100 nm range at least in one dimension.[15] In Figure 1.1, the size difference of nanoparticles with other molecules and materials is given. The field of science that deals with nanoparticles is called nanoscience and it has produced many new materials that have useful chemical and physical properties. Depending on their size, morphology, and chemical composition, variety of nanoparticles such as metal nanoparticles,[11,12,16–20] carbon-based nanoparticles,[13,21,22] semiconductor nanoparticles,[23–26]ceramic nanoparticles,[27,28] polymeric nanoparticles,[29] and lipid-based nanoparticles can be obtained.[30]
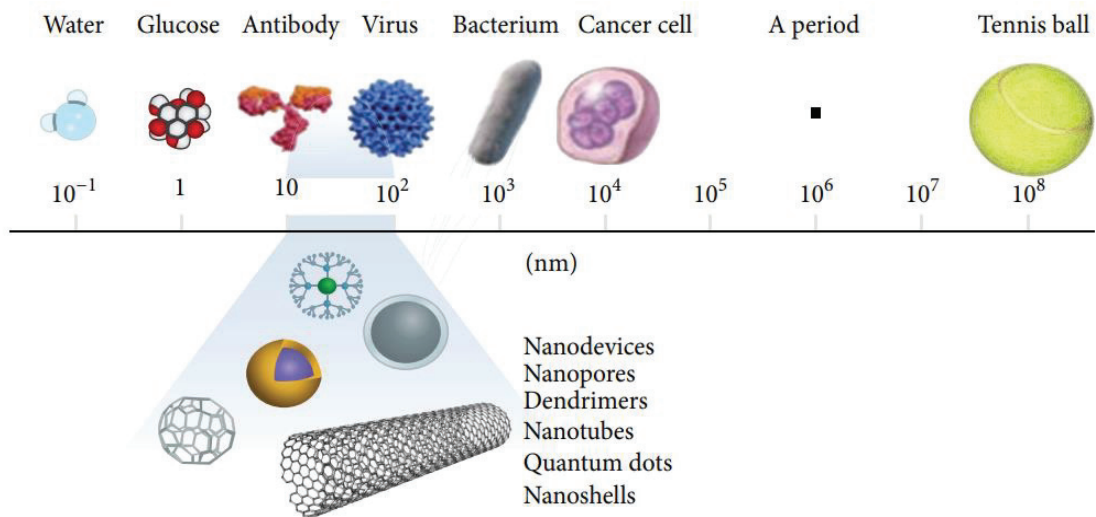
Figure 1.1. Size of nanoparticles with respect to other materials.[1]

There are two ways to synthesize nanoparticles, one is the bottom-up approach and the other is the top-down approach. The bottom-up approach focuses on the usage of chemical and physical forces at the nanoscale dimension to assemble basic units into nanoparticles whereas the top-down approach is the destructive approach that contains the breakage of bulk material into nanoscale dimensions.

The reason why nanoparticles get so much attention is that the material properties change as their size approaches to the nanoscale dimension. When the optical, electrical, mechanical, magnetic, and catalytic properties of nanoparticles are compared with their bulk counterparts, many differences can be easily detected. Generally, at nanoscale dimension, color changes; electric and magnetic properties are enhanced; hardness increases; inert materials become efficient chemical catalysts. As materials are shrunk, their volume decreases faster with respect to the surface areas, thus increasing the surface area-to-volume ratio. One of the most important features that make nanoparticles special is that they have a very large surface area-to-volume ratio. The use of nanoparticles is even older than we think. Nanoparticles have been used knowingly or unknowingly for a long time. The best example of this is the colored windows in the churches (Figure 1.2). The nanoparticles have found a place for themselves in many industries such as textile, cosmetics, electronics, pharmaceuticals, and even food.

2

Figure 1.2. One of the windows of the Votive Church, Vienna

.

1.1.1. Metal Nanoparticles

Metal nanoparticles are synthesized by using metal oxides or metal salts. Metal ions are reduced to metal atoms and these atoms self-assemble into nanoparticles in any shape by chemical and physical forces at nanoscale dimension. The metal core is covered with inorganic or organic molecules or metal oxides. Ever since Michael Faraday conducted research on colloidal gold and published his famous paper "Experimental relations of gold (and other metals) to light"[31] in the 1800s, noble metal nanoparticles such as gold, silver, platinum, and copper have been an important research topic. So far, we have witnessed many different metal nanoparticle morphologies such as triangular nanoprisms,[32] nanorods,[33] nanocubes,[34] nanocages,[35] nanodisks,[11] and nanostars,[17,36] nanodecahedrals,[12] nanowires,[18,37] and hollow nanostructures[20] (see Figure 1.3). These metallic particles can be obtained by using various methods such as lithography (top-down approach) and wet chemistry (bottom-up approach).

3
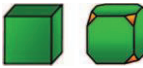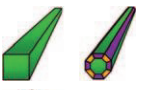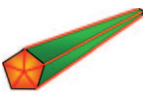
Structures	Shapes	Schematic drawings	Metals
single-crystal	perfect/truncated cube[a]		Pd, Ag, Au, Pt, Cu, Rh, Bi, Fe
	perfect/truncated octahedron[a]		Pd, Ag, Au, Pt
	perfect/truncated tetrahedron[a]		Ag, Au, Pt, Rh
	rectangular bar		Pd, Ag, Pt
	octagonal rod		Pd, Au, Fe, Co, Ni
	rectangular or octagonal wire		Pb, In, Sn, Sb, Fe, Co
singly twinned	right bipyramid		Pd, Ag
	beam		Ag
multiply twin-ned	decahedron[a]		Pd, Ag, Au
	icosahedron[a]		Pd, Au
	five-fold twinned pentagonal rod		Pd, Ag, Au, Cu
	five-fold twinned pentagonal wire		Ag, Au, Cu
	triangular/hexagonal plate		Pd, Ag, Au, Cu, Pb, Bi, Co, Ni
	disc		Sn, Co

Figure 1.3. Different shapes of metal nanoparticles.[2]

The most attractive synthesis method of metal nanoparticles is using wet chemistry because, in this method, a large number of nanoparticles can be synthesized in colloidal form. In addition, the size and shape of nanoparticles are tuned by changing reaction ingredients. Metal ions, complexing agents, weak and strong reducing agents are all used in the colloidal synthesis of metal nanoparticles, and the associated colloidal synthesis of metal nanoparticles is frequently activated and accelerated by heat, light, or, in certain situations, a reducing agent. Photoinduced techniques, for example, have been utilized to change the shape of the metal nanoparticles by using visible and ultraviolet light sources.

Metal nanoparticles like gold and silver possess different optical, electrical, mechanical, magnetic, catalytic properties from their bulk counterparts. The color of any

material depends on how the material interacts with the incoming light. When the incident light interacts with material, the amount of light reflected, scattered, absorbed, and transmitted determine the color we see, and it is unique to the material itself. If you have several gold coins and bars of different sizes, all of them will be gold in color. Similarly, if you have several silver coins and bars with different sizes, all of them will be silver in color. However, if the size of gold approaches to nanoscale (aorund 100 nm), the size of the nanoparticle is now comparable with the wavelength of the incident light. Then, when light interacts with gold nanoparticles, the amount of light reflected, scattered, absorbed, and transmitted not only depends on the material but also on the size, shape, and the surrounding medium (refractive index) of the nanoparticles. This is exactly why we can see nano-sized nobel metals in different colors (Figure 1.4.).
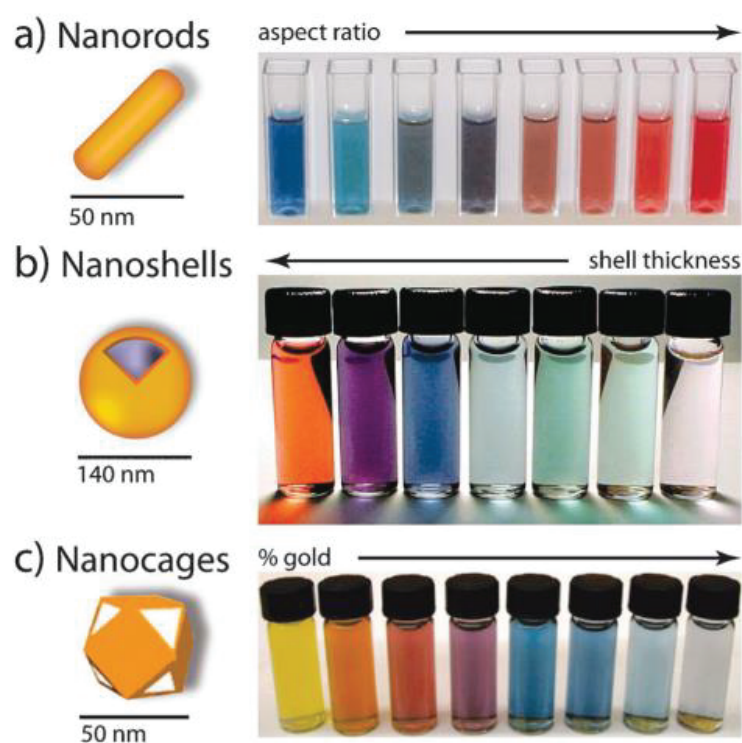
Figure 1.4. Color change of the gold nanoparticles with size and shape.[3]

Metal nanoparticles embody many free electrons. These free electrons oscillate collectivelly. Quantum of these free electron oscillations are called plasmons or mainly surface plasmons (SPs). When incident light impinges on the surface of the metal nanoparticles, their free electrons interact strongly with the electric field of the incident

light at the metal-dielectric interface and hence surface plasmon polaritons (SPPs) are formed. The plasmonic properties of these metal nanoparticles will be discussed in detail in part 1.2. Controlling the dimensions and shape of the metal nanoparticles has always been the focus of initiatives in this area. Thanks to their unique optical properties, metal nanoparticles have been involved in many applications such as combining photonics and electronics at nanoscale dimension.[38–40]

1.1.2. Carbon Quantum Dots

Carbon quantum dots (CDs) are fluorescent semiconductor nanocrystals having zero-dimension (less than 10 nm in size). In fact, CDs were discovered by chance during the purification of carbon nanotubes by preparative electrophoresis in 2004.[41] To be able to synthesize CDs, both bottom-up and top-down approaches have been widely employed. Hydrothermal, solvothermal, and microwave synthesis of CDs from organic precursors [13,42,43] are the most commonly used synthesis strategies along with laser ablation of graphite powder,[44] electrochemical conversions of carbon nanotubes into CDs,[45] separations of impurities (carbon quantum dots) from arc-synthesized single-walled carbon nanotubes.[41] However, the bottom-up approach has caught more interest than the top-down approach because by using the bottom-up approach, the degree of carbonization of CDs can be affectively tuned.

Photoluminescence behaviors of CDs are strongly dependent on excitation, solvent, and the pH of the solvent. In spite of the fact that the size of the CDs, surface chemical groups, and doping atoms may explain the photoluminescence (PL) behavior, there is no widespread assertion on the particular PL mechanism.[46] CDs show excitonic transitions in the visible region. When photons with energy higher than the energy of the bandgap of the material, excitons are generated.[47] Electrons are elevated from the valence band to the conduction band. As a result, a positively charged hole is left by the negatively charged electron. This electron-hole pair is named as an exciton.

CDs are nominated instead of fluorescent dyes and traditional cadmium and lead-based semiconductor quantum dots due to their low cost, photostability, chemical inertness, biological friendly, low toxicity, water-solubility, bright and strong luminescence, ease of functionalization, and simple synthesis. Therefore, there have been a rapid increase in the carbon quantum dots (CDs) and their successful applications in optoelectronic devices,[48] photodynamic therapy,[49] drug delivery, and bioimaging.[50]

1.2. Surface Plasmon Polaritons

Collective oscillations of electron density in a conducting medium such as a metal is known as plasma oscillations. The quantum of plasma oscillations is called plasmon. When incident photons interact with surface plasmons of metal surface, surface plasmon polaritons (SPPs) are formed in the strong coupling condition. SPPs, which are hybrid state of electron and photon, are at the metal-dielectric interface (see Figure 1.5). First discovered by Rufus Ritchie[51] in 1957, surface plasmon polaritons were extensively studied by many well-known scientists such as E. Kretschmann, E. N. Economou, Heinz Raether.
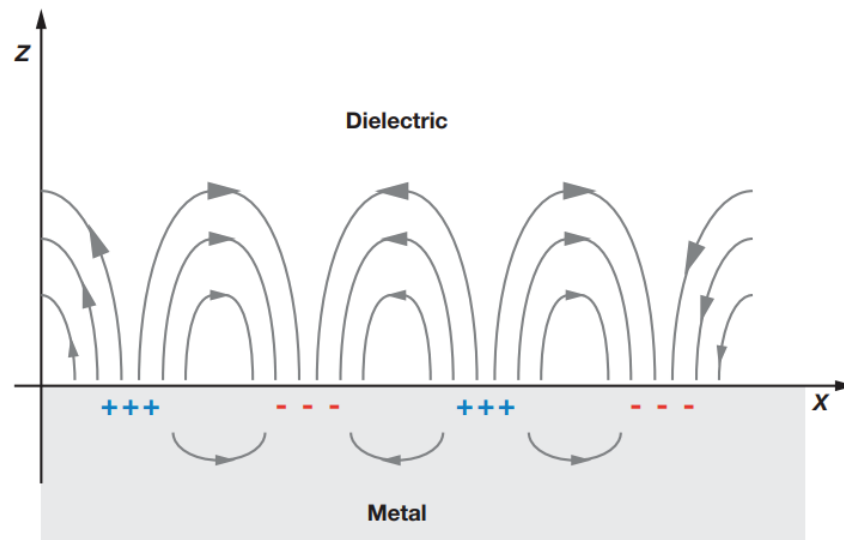
Figure 1.5. Surface plasmon polaritons (SPPs) on a metal-dielectric interface.[4]

Metal nanoparticles and metal thin films support surface plasmon polaritons. When photon impinges on the surface of the metal nanoparticles, the electric field of the incident photon interacts with the free electrons on the surface of the metal nanoparticles. This resonant oscillation is called surface plasmon resonance (SPR). The plasmon resonances of metal nanoparticles of silver and gold can be in the visible range of the electromagnetic spectrum. If they are illuminated with a white light, gold and silver nanoparticles absorb incident light when the incident light is in resonance with the surface plasmon frequency.

Light can be confined and guided by metal nanoparticles in subwavelength regions. Localized surface plasmon polaritons (LSPPs) are electron density oscillations locally around the metal nanoparticle (see Figure 1.6).
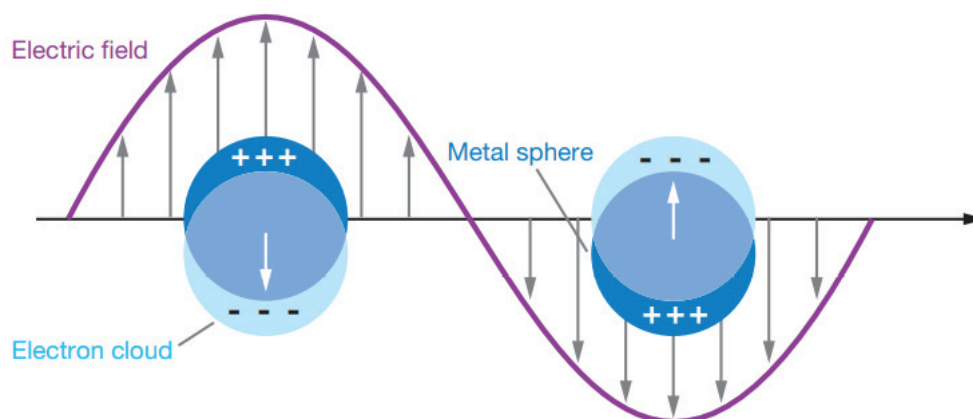
Figure 1.6. A localized surface plasmon polariton in a metal nanoparticle.[4]

When localized surface plasmons interact with incident photons, localized surface plasmon polaritons (LSPPs) are generated. In LSPP, the formation of a dipole in the metal nanoparticle is caused by the electric field of the incident photon, whereas the restoring forces try to eliminate this formation. Therefore, only the frequency of visible light which is resonant with the collective oscillation of free electrons of metal nanoparticles is absorbed.

SPPs are easily affected by the change in the shape and size of the metal nanoparticles as well as the change in the refractive index of the environment in which they are dispersed.[52] Thus, if any of these parameters change, the resonance frequency of SPPs can be tuned. SPPs have demonstrated themselves in many application areas such as solar cells, sensors, microscopy, light-emitting diodes, nano-optics, and surface-enhanced spectroscopy.[53–55]   In this thesis, silver nanodisks, decahedral silver nanoparticles, decahedral bimetallic (silver & gold) nanoparticles, and silver thin films are used in order to generate SPPs.

When surface plasmons on the metal thin films and incoming photons are in resonance, SPPs can be generated. To be able to excite SPs on the surface of the metal thin films, photons cannot be utilized directly owing to the momentum mismatch.[5] To defeat

momentum mismatch, special arrangements are required. Excitation of surface plasmons on metal thin films is achieved by Kretschmann configuration,[56] Otto configuration,[57] or diffraction grating.[58] Figure 1.7 shows the different types of special arrangements. Among them, Kretschmann configuration is mostly the preferred method.[59] In the Kretschmann configuration, a glass prism is used to increase momentum of the incident photon in order to achieve excitation of SPPs. In this study, for the excitation of SPPs on metal thin films, Kretschmann configuration has been used.
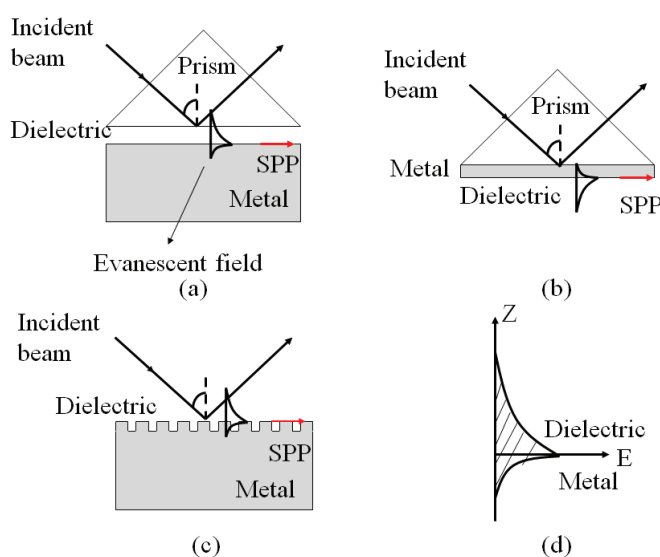
Figure 1.7. Surface plasmon resonance: (a) Otto configuration, (b) Kretschmann configuration, (c) a diffraction grating, and (d) an evanescent field at the interface.[5]

1.3. Excitons

Semiconductor and insulator materials have a bandgap while metals do not have a bandgap. In order to generate excitons, semiconducting materials must be excited by photons with an energy higher than the energy of the bandgap of the semiconductor material.[60] When semiconductors or insulators are excited by photons that have higher energy than their band gaps, electrons are elevated by the energy absorbed from incoming photons and electrons go to the conduction band, hence a positively charged hole is left behind the negatively charged electron. This hole-electron pair is called an exciton and is electrically neutral. The positive and negative charges are attracted to each other coulombically. The first scientist to mention the exciton was Yakov Frenkel in 1931.[61]

There are two types of excitons due to the strength of electron-hole binding; one is Frenkel and the other is Wannier-Mott excitons (see Figure 1.8)
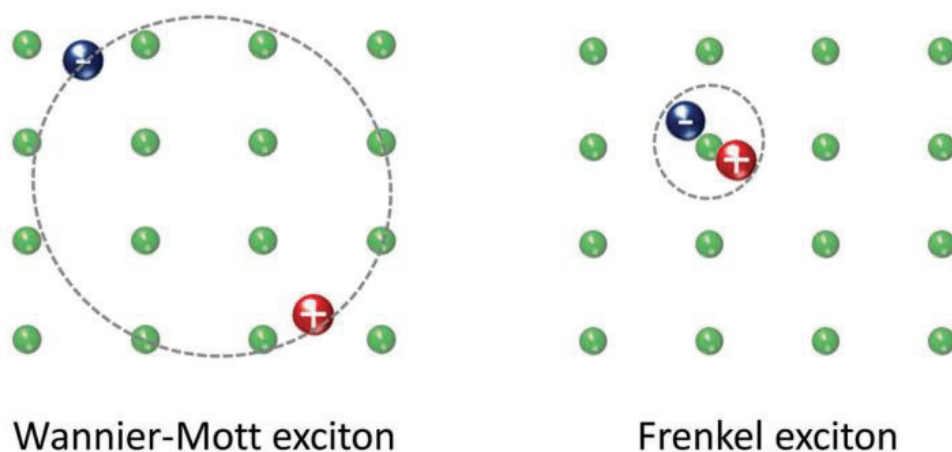
Figure 1.8. Schematic illustration of representative exciton models.[6]

Frenkel excitons can be found in materials that have a comparably small dielectric constant in which the Coulombic interaction between hole and electron tends to be strong thus exciton Bohr radius is small, which leads to excitons to be small[62]. Besides, the binding energy of Frenkel excitons is between 0.1-1.0 eV.[63] Frenkel excitons can be found in organic semiconducting materials.[61] J-aggregate dyes are the most commonly used Frenkel excitons.

Wannier-Mott excitons can be found in materials that have large dielectric constants in which the Coulombic interaction between hole and electron is decreased as a result of electric field screening thus exciton Bohr radius is large.[62]Wannier-Mott excitons are named by Swiss physicist Gregory Wannier[64] and British physicist Nevill Francis Mott. The binding energy of the Wannier-Mott excitons is ~0.01 eV.[63] Wannier- Mott excitons can be observed in inorganic semiconducting materials.[61] Nowadays, halide perovskites, [65] quantum dots (QDs),[66] and CdSe nanoplatelets[67] are used as the source of Wannier-Mott excitons.

In this thesis, J-aggregate dyes and carbon quantum dots (CDs) are used as source of exciton. In 1937, J-aggregate dyes were firstly introduced by Scheibe[68] and Jelley.[69] These organic molecules have the ability to self-assemble at high concentrations. At high concentration, the dye monomers self-assemble into dimers and then the brick wall-like

structure. Strong π-π interactions between the molecules result in reversible aggregation of dye molecules.[70,71] The chemical structure of cyanine dye C8S3 is given in Figure 1.9.

The absorption bands of dye monomers shift to shorter or longer wavelengths by aggregation of the molecules and are also narrowed (see Figure 3.3). In fact, the molecular aggregates can be categorized as H-aggregates, and J-aggregates owing to the geometry
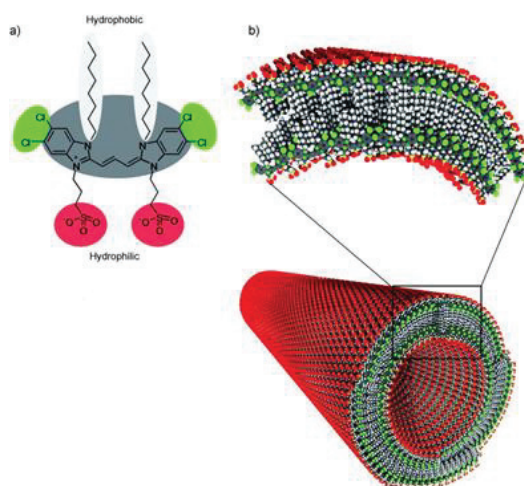
Figure 1.9. a) Chemical structure of cyanine dye C8S3. b) A model of double-walled nanotube of C8S3.[7]

of the molecular arrangement.[72] The geometry of the molecular arrangement of J-aggregates and H-aggregates are shown in Figure 3.3. The dye monomers stick face to face in H-aggregates and absorption bands of the H-aggregates shift to shorter wavelengths because the electronic state is at higher energy whereas, in J-aggregates, monomers follow the edge to edge aggregation or in other words head to tail configuration and the absorbance bands of the J-aggregates shift to longer wavelengths because the electronic state is at lower energy (Figure 1.10).[9]

The electronic band structure of these dye molecules can be modified by different geometric formations. Strong intermolecular π electronic coupling occurs because of the packing of the aggregates.[72] Delocalization of electronic states is increased in aggregates owing to the alignment of the monomers.[73]
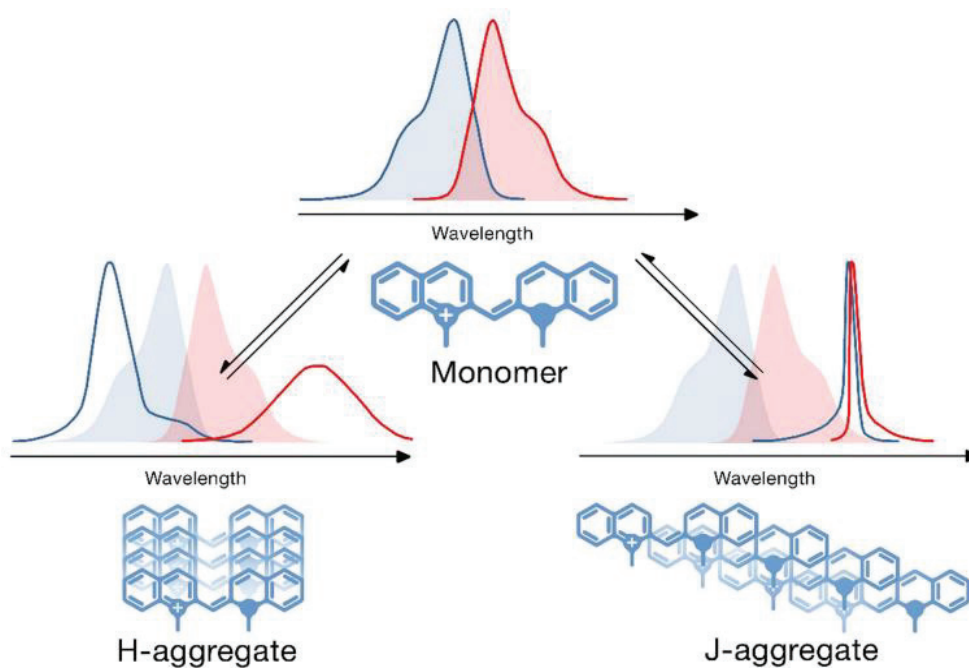
Figure 1.10. Schematic representation of the formation of H- and J-aggregates.[8]

Owing to their electronic and optical properties, J-aggregates have attracted great attention. They can act as a light-harvesting system based on chlorophyll.[73] Among J-aggregates, cyanine dyes are well known such as 5,5′,6,6′-tetrachlorodi(4-sulfobutyl) benzimidazolocarbocyanine (TDBC). In this thesis, TDBC is used as J-aggregate dye to synthesize colloidal plexcitonic nanoparticles.
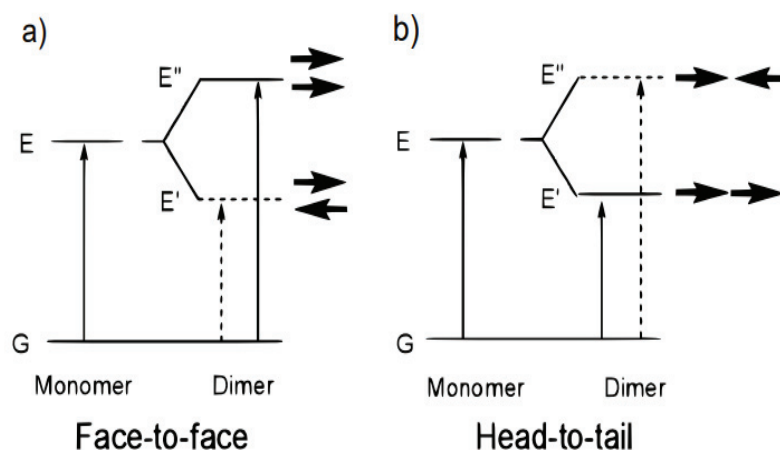
Figure 1.11. a) Face to face stacking of monomers to form H-aggregates. b) Head to tail stacking of monomer to form J-aggregates.[9]

1.4. Plexcitons

Plexcitons are hybrid states that result from the interaction between plasmons of metal nanoparticles or metal thin films and excitons of molecules or quantum dots (see Figure 1.12).[74] Plexcitons have received interest owing to their ease of synthesis, scalability, and ability to provide sub-wavelength confinement and hence they offer promising applications.[75] The first plexcitonic nanoparticles, which are a complex of gold nanoshell and J-aggregate, were synthesized by N. J. Halas et al.[74] in 2008. Plexcitonic particles can be produced by using lithographic techniques and wet chemistry methods to study the plasmon-exciton interaction. Plexcitons show half-plasmonic and half-excitonic character. The interaction between plasmons and excitons is divided into two; one is strongly coupled system where interaction between plasmons and excitons is strong and another is weakly coupled system where the interaction between plasmons and excitons is weak.
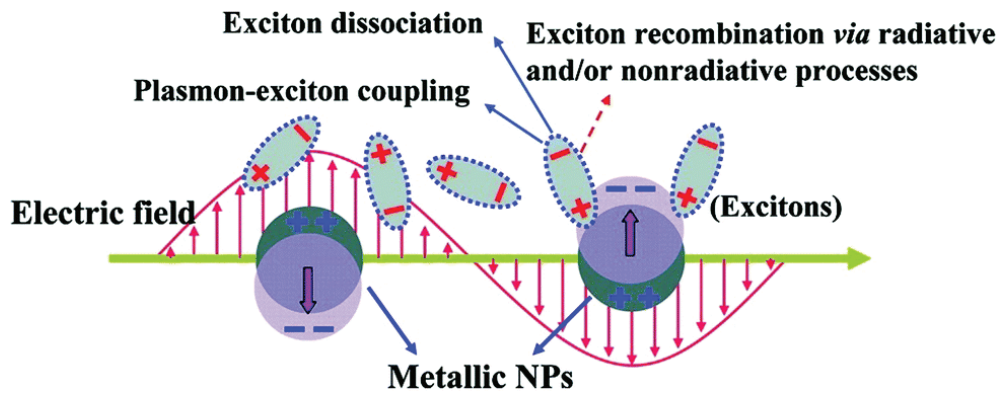
Figure 1.12. Schematic representation formation of plexcitonic nanoparticles.[10]

When metal nanoparticles meet with the excitonic source, their resonance overlaps thus leading to the splitting of the original absorption band of the metal nanoparticle (see Figure 4.2). This separation between upper and lower branches is known as vacuum Rabi splitting.[76] In such systems, there is a reversible energy flow between plasmon and exciton. The Rabi splitting energy yields information about the coupling strength and the amount of energy exchanged between plasmon and exciton.[10]
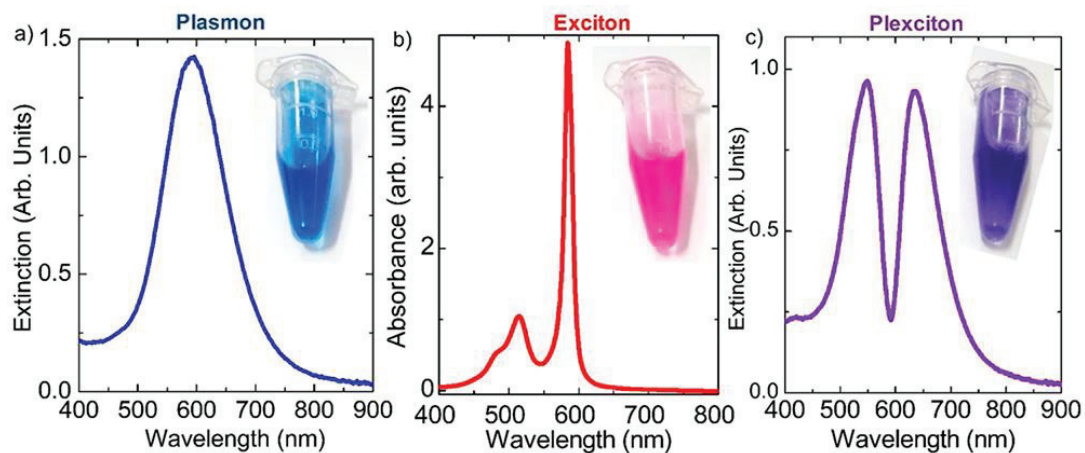
Figure 1.13. a) Extinction spectrum of disk shaped silver nanoplate colloid in water. b) Absorption spectrum of TDBC dye in water. c) Extinction spectrum of disk shaped plexcitonic nanoparticle colloid.[11]

1.5. Liquid Crystals (LCs)

In general, matter can be found in three main states; these are solid, liquid, and gas states. From the past to the present, scientists discovered new intermediate states of matter such as liquid crystals. When liquid crystals are discovered by two scientists Friedrich Reinitzer[77] and Otto Lehmann,[78] solid, liquid, and gas were known as the three main states of matter. Liquid crystal is a well-known intermediate state of matter in which the properties of the liquid phase and the solid phase are combined. Due to its dual character, liquid crystal phases are known as mesophase or mesomorphic phases.[79] At certain temperatures, some materials become liquid crystalline, which means they tend to flow like a liquid but have some of the optical properties of a solid due to the ordered arrangement of their molecules. Liquid crystals can be grouped according to their different optical properties such as texture.

In general, liquid crystals are divided into two according to the method of obtaining the phase; these are lyotropic and thermotropic liquid crystals. To obtain the lyotropic liquid crystal phase, the solvent is varied whereas for having thermotropic liquid crystal phase, the temperature is changed. In this thesis, lyotropic liquid crystal mesophases are used to confine CDs into spaces for studying plasmon-exciton coupling on the metal thin film.

To achieve lyotropic liquid crystal (LLC) mesophases, amphiphilic molecules (molecules that have hydrophilic head and hydrophobic tail) are dissolved in solvent under suitable temperatures. The amount of solvent added and as well as the amount of amphiphilic molecule dissolved play a vital role in the formation of the phase. The LLCs are classified as lamellar, hexagonal, and micellar cubic phases structurally. Lyotropic liquid crystals have a bright future owing to their unique properties and played important role in many application areas such as biology, food science, photonics, electronics, pharmacy, etc. For instance, they are used as gel-electrolytes for optical modulators,[80] and solar cells,[81] as media for the synthesis of CDs,[82], and as a potential drug delivery system.[83]

CHAPTER 2

MATERIALS AND METHODS

2.1. Experimental Methodology

2.1.1. Synthesis of Colloidal Nanodisk Shaped Plexcitonic Nanoparticles

During the whole experimental procedure and characterization, Milli-Q water with a resistivity of 18.2 MΩ cm was utilized. L-Ascorbic acid (C6H8O6), trisodium citrate dihydrate (TSC), poly(sodium 4-styrenesulfonate) (PSS), silver nitrate (AgNO$_3$), and sodium tetraborate (NaBH$_4$) were purchased from Sigma Aldrich. 5,5',6,6'-Tetrachlorodi(4-sulfobutyl)benzimidazolocarbocyanine (TDBC) dye was purchased from FEW Chemicals GmbH. All reagents were used without purification.

The synthesis of spherical silver nanoparticles was conducted in an aqueous medium at room temperature. All solutions required for synthesis were freshly prepared. The synthesis steps proceed as follows. 5 mL of 2.5 mM TSC solution was transferred to a glass vial containing a magnetic stirring bar. After that glass vial containing TSC solution was placed on the magnetic stirrer. Then, 0.25 mL of 500 mg/L poly(sodium 4-styrenesulfonate) (PSS) and 0.3 mL of 10 mM NaBH$_4$ were added to solution mentioned above. In the final step, about 2mL per minute to be dropped, 5 mL of 0.5 mM AgNO$_3$ was introduced dropwise to this mixture. In approximately, 30 minutes, a yellow-colored solution along with the plasmon resonance wavelength around 400 nm, which indicates the formation of spherical silver nanoparticles, was achieved. For further use, the yellow-colored seed solution was covered by aluminum foil in order to protect the solution from sunlight exposure and aged about overnight to be able to decompose the excess reducing agent which is NaBH$_4$.Yellow-colored spherical silver nanoparticles were used as seed solution in order to synthesize silver nanoprisms.

As in the synthesis of spherical silver nanoparticles, the synthesis of silver nanoprisms was conducted in aqueous environment at room temperature. To synthesize silver nanoprisms, spherical silver nanoparticles were utilized as seed solutions. Typical seed-mediated growth of silver nanoprisms was achieved as follows.[84,85] First of all, 5mL Milli-Q water was transferred to glass vial containing magnetic stirring bar. After that 75 µL of 10 mM ascorbic acid was added in 5mL water and continued with the addition of different amounts of seed solution, e.g., 60 µL, depending on desired size of silver nanoprisms. About 1mL per minute to be dropped, 0.5 mM $AgNO_3$ was introduced dropwise to this reaction mixture right after the addition of seed solution. Upon addition of $AgNO_3$ solution, the color of the reaction mixture changes due to the amount of seed solution present. Finally, 0.5 mL of 25 mM TSC solution was added to stabilize the newly formed silver nanoprism. Glass vials containing silver nanoprisms were covered with aluminum foil and stored for further use. There was no need for purification for further use.

The shape conversion method was used to synthesize silver nanodisks. To do this, nanoprisms were heated as in previous studies.[86] The newly synthesized silver nanoprisms, which do not require purification, were placed in an oil bath and heated at 95 °C for 2 hours under stirring. Upon heating, the color of the silver nanoparticle solutions changed. After the heating procedure, the silver nanodisk solutions were removed from the oil bath and allowed to reach room temperature in the dark. After reaching room temperature, silver nanodisk solutions were covered with aluminum foil and stored for further use.

To synthesize plexcitonic nanoparticles, there is a need for plasmon and exciton sources. In here, silver nanodisks were used as plasmon sources while 5,5′,6,6′-tetrachlorodi(4-sulfobutyl)benzimidazolocarbo-cyanine (TDBC) was used as the source of exciton. TDBC was used without any purification whereas silver nanodisk solutions were centrifuged at 15 000 rpm for 15 min to remove sideproduct, supernatants were discarded and pellets were redispersed in water. After that 0.1 mM TDBC solution was prepared. Then, plexcitonic particles were synthesized as follows. First of all, different amounts of 0.1 mM TDBC solution, e.g 10 and 100 µL, were introduced to silver nanodisk solution under stirring. After the addition of TDBC, the color of the solutions changed, which is a strong indication of the formation of plexcitonic nanoparticles. In order to get rid of excess dye molecules in the solution, nanodisk shaped plexcitonic nanoparticles were centrifuged 15 000 rpm for 15 min. Finally, the supernatants were removed and the

pellets were redispersed in water. Nanodisk shaped plexcitonic nanoparticles were covered with aluminum foil and stored for spectroscopical characterization.

2.1.2. Decahedral Shaped Ag Nanocrystals and Strong Light- Matter Coupling in Decahedral Ag-Au Alloyed Nanocrystals

In this subsection of the thesis, the laser-assisted synthesis of anisotropic silver nanocrystals and strong light-matter coupling in silver-gold alloyed nanocrystals are given.

During the whole experimental procedure and characterization, Milli-Q water with a resistivity of 18.2 MΩ cm was utilized. Polyvinylpyrrolidone (PVP) (40000), trisodium citrate dihydrate (TSC), L-Arginine, silver nitrate (AgNO$_3$), HAuCl4, sulfuric acid (H2SO4) (95%), hydrogen peroxide (H2O2) (30%), 16-mercaptohexadecanoic acid (90%), (3-aminopropyl)trimethoxysilane (97%) and sodium tetraborate (NaBH$_4$) were purchased from Sigma Aldrich. 5,5',6,6'-Tetrachlorodi(4-sulfobutyl)benzimidazolocarbocyanine (TDBC) dye was purchased from FEW Chemicals GmbH. All reagents were used without purification. For plasmon-plasmon coupling index matching fluid, a glass prism made of BK7 and supercontinuum laser (Koheras-SuperK Versa) with a spectral width of around 1 nm were used. Blue laser at 488 nm was purchased from CrystaLaser.

The synthesis of spherical silver nanoparticles was conducted in an aqueous medium at room temperature. All solutions required for synthesis were freshly prepared. The synthesis steps proceed as in the previous study.[87] First of all, 7 mL of Milli-Q water was transferred to glass vial containing magnetic stirring bar and this glass vial was placed on the magnetic stirrer. It was followed by the addition of 0.5 mL of 50 mM TSC and 15 μL of 50 mM PVP (40000), respectively. After that 200 μL of 5 mM AgNO$_3$ was introduced to this mixture. 80 μL of 100 mM NaBH$_4$ was added this mixture to reduce the silver ions present. Finally, 50 μL of 5 mM L-Arginine was added which is used as a photochemical promoter. The yellow-colored solution was allowed to stir for several minutes. The resulting yellow color of the colloid indicates the formation of spherical silver nanoparticles, which have localized SPP resonance wavelength at around 400 nm.

The synthesis of decahedral shaped silver nanoparticles was conducted in an aqueous medium at room temperature under magnetic stirring. To be able to synthesize

decahedral shaped silver nanoparticles, previously synthesized spherical silver nanoparticles was taken into a dark room and irradiated by blue laser at 488 nm (50 mW, CrystaLaser) for nearly 15 h. In the final step, the resulting solution was centrifuged at 5000 rpm for 15 minutes. The supernatants, which contain byproducts, were removed while the pellets were redispersed in water for further use. The resulting solution was covered by aluminum foil.
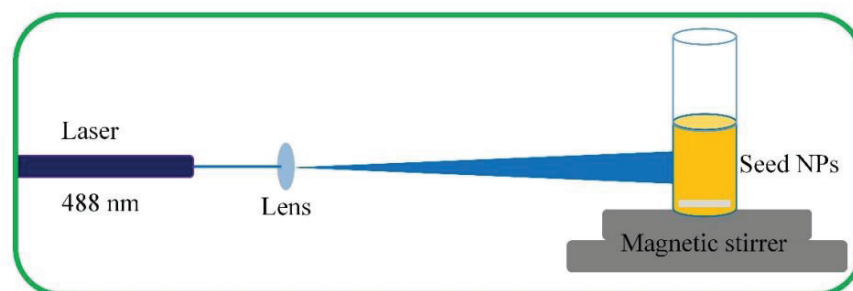
Figure 2.1. Schematic representation of the synthesis of decahedral shaped silver nanoparticles conducted in an aqueous medium at room temperature under magnetic stirring by blue laser at 488 nm.[12] Reprinted with permission from Balci, F. M.; Sarisozen, S.; Polat, N.; Guvenc, C. M.; Karadeniz, U.; Tertemiz, A.; Balci, S. Laser Assisted Synthesis of Anisotropic Metal Nanocrystals and Strong Light-Matter Coupling in Decahedral Bimetallic Nanocrystals. Nanoscale Advances 2021, 3 (6) https://doi.org/10.1039/d0na00829j. Copyright 2021 Royal Society of Chemistry.

The synthesis of silver-gold bimetallic nanoparticles was conducted in an aqueous medium at room temperature under magnetic stirring. The synthesis steps proceed as follows. First of all, 4 mL of laser-assisted synthesized decahedral silver nanoparticles were centrifuged two times at 5000 rpm for 15 minutes. The supernatants were removed while the pellets were redispersed in 1 mL of water. Then, 100 ml of 50 mM of TSC was introduced to solution of decahedral silver nanoparticles for stabilization. It was followed by the dropwise addition of 50 μL of 50 mM HAuCl4 solution several times to achieve silver-gold bimetallic nanoparticles. Upon the addition of HAuCl4, galvanic replacement reaction between silver atoms and gold ions started, and bimetallic nanoparticles were formed. In the final step, bimetallic nanoparticles were centrifuged at 15000 rpm for 10 min and the pellets were redispersed in water. The resulting solution was covered by the aluminum foil for further use.

To synthesize plexcitonic nanoparticles, there is a need for plasmon and exciton sources. In here, silver-gold bimetallic decahedral nanoparticles were used as plasmon sources while 5,5′,6,6′-tetrachlorodi(4-sulfobutyl)benzimidazolocarbo-cyanine (TDBC) was used as the source of exciton. TDBC was used without any purification. Silver-gold bimetallic decahedral nanoparticles centrifuged and dispersed in water in the previous step were combined with different amounts of 0.1 mM TDBC, e.g 10 and 100 μL, under stirring at room temperature. The resulting mixture was covered by aluminum folie and incubated overnight. Afterward, the incubated mixture was centrifuged at 15 000 rpm for 10 min to remove uncoupled TDBC molecules. The supernatant was removed whereas the pellet was redispersed in water. The resulting solution was covered by aluminum foil.

Plasmon-plasmon coupling or hybridization between decahedral shaped bimetallic nanoparticles and the flat metal thin film was achieved by Kretschmann configuration.[88]To prepare flat silver thin films with the thickness of 40 nm, the following procedure was conducted. First of all, the glass microscope slides were cleaned with a piranha solution. Piranha solution was prepared by combining 3:1 ratio of sulfuric acid (95%) and hydrogen peroxide (30%). After that cleaned glass microscope slides were coated by thermal evaporation of silver with a purity 99.9 % under vacuum. Thereafter, the surface of the prepared flat silver thin films was chemically modified by using 16-mercaptohexadecanoic acid (90%) and (3-aminopropyl)trimethoxysilane (97%). To do this, 10 mM 16-mercaptohexadecanoic acid (90%) was prepared in 10 mL isopropanol and silver thin films were dipped into this solution for 30 minutes. It was followed by the washing of silver thin films with isopropanol. After that modified silver thin films were dipped into 30 mM (3-aminopropyl)trimethoxysilane (97%) in isopropanol for 30 minutes. It was followed by washing of silver thin films with isopropanol and water. Silver thin films were dried. Then, bimetallic decahedral nanoparticles were coated on the surface of the silver thin film by spin-coater and electrostatically self-assembled on the modified surface of the silver thin film. Afterward, bimetallic decahedral nanoparticles coated silver thin films were put on the glass prism made of BK7 which contained index matching fluid. Index matching fluids reduce unwanted optical reflections. Surface plasmons of silver thin films were excited by utilizing glass prism made of BK7 and a tunable laser light source, which was supercontinuum laser (Koheras-SuperK Versa) with a spectral width of around 1 nm. Thus, localized SPPs of metal nanoparticles and propagating SPPs of Ag thin film are coupled.
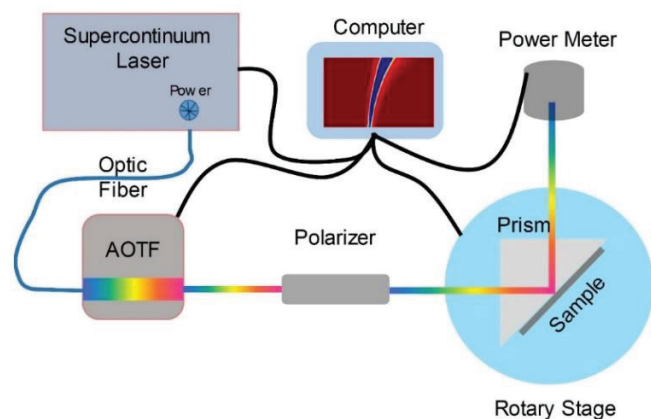
Figure 2.2. The experimental setup utilized to couple localized surface plasmon polaritons of Ag-Au bimetallic decahedral shaped nanoparticles with propagating surface plasmon polaritons of flat Ag thin film is depicted schematically.[12] Reprinted with permission from Balci, F. M.; Sarisozen, S.; Polat, N.; Guvenc, C. M.; Karadeniz, U.; Tertemiz, A.; Balci, S. Laser Assisted Synthesis of Anisotropic Metal Nanocrystals and Strong Light-Matter Coupling in Decahedral Bimetallic Nanocrystals. Nanoscale Advances 2021, 3 (6) https://doi.org/10.1039/d0na00829j. Copyright 2021 Royal Society of Chemistry.

2.1.3. Strong Coupling of Carbon Quantum Dots in Liquid Crystals

During the whole experimental procedure and characterization, Milli-Q water with a resistivity of 18.2 MΩ cm was utilized. L-Phenylalanine, o-Phenylenediamine (OPD), sodium hydroxide (NaOH), sulfuric acid (H2SO4) (95%), hydrogen peroxide (H2O2) (30%), decaethylene glycol mono-dodecyl ether were purchased from Sigma Aldrich. 5,5',6,6'-Tetrachlorodi(4-sulfobutyl)benzimidazolocarbocyanine (TDBC) dye was purchased from FEW Chemicals GmbH. All reagents were used without purification. For plasmon-exciton coupling index matching fluid, a glass prism made of BK7 and supercontinuum laser (Koheras-SuperK Versa) with a spectral width of around 1 nm were used.

A hydrothermal method was used to synthesize carbon quantum dots at high temperatures and under high pressure. To do this, 8 mL of Milli-Q water was transferred to 25 mL Teflon-lined stainless-steel autoclave containing magnetic stirring bar. Afterward, Teflon-lined stainless-steel autoclave was placed on the magnetic stirrer. It was followed by the addition of 0.0991 g (0.6 mmol) of L-Phenylalanine and 0.0649 g (0.6

mmol) of o-Phenylenediamine. Then, 2 mL of sulfuric acid (95%) was introduced to this mixture. Upon addition of sulfuric acid, the solubility of chemicals added was increased significantly. The mixture was allowed to stir for the complete dissolution of the chemicals in an 8:2 mixture of Milli-Q water and sulfuric acid. After dissolving the chemicals, the resulting solution was transparent in color. Subsequently, the magnetic stirring bar was removed from the Teflon-coated stainless-steel autoclave. The Teflon-lined stainless-steel autoclave was then placed in a preheated oven at 210°C. The reaction took 12 hours to complete. After 12 hours, the Teflon-coated stainless-steel autoclave was removed from the oven and allowed to cool. The solution color at the end of the reaction was observed as dark blue. Subsequently, the dark blue colored solution was centrifuged at 15000 rpm for 15 minutes. Precipitated large aggregates were removed whereas the supernatant was filtered by a 0.22 μm syringe filter. After that NaOH solution was prepared in water. Meanwhile centrifuged and filtered dark blue colored CD solution was diluted with Milli-Q water. NaOH solution was introduced drop by drop in diluted dark blue colored solution in order to precipitate CD under stirring. The addition of NaOH continued until pH reached 7. In order to discard the excess amount of NaOH, the neutralized solution was centrifuged three times at 15000 rpm for 15 min. In each centrifugation, the supernatant was removed and the pellet was redispersed in water. In the end, the pellet was left to dry for further use and characterization.

In order to prepare LLC mesophases, sulfuric acid (SA) / Polyoxyethylene (10) lauryl ether (C12E10) having a mole ratio of 2.5 was used as a solution in ethanol. Then, this solution was dropped on the glass microscope slide. When ethanol evaporated, the gel phase formed. The gel phase on the glass microscope slide showed hexagonal texture under the polarized optical microscope.

Plasmon-exciton coupling between SPPs of silver thin film and excitons of CDs was achieved by utilizing Kretschmann configuration. To prepare flat silver thin films with the thickness of 25, 50 and 60 nm following procedure was conducted. First of all, the glass microscope slides were cleaned with piranha solution. Piranha solution was prepared by combining a 3:1 ratio of sulfuric acid (95%) and hydrogen peroxide (30%). After that cleaned glass microscope slides were coated by thermal evaporation of silver with the purity 99.9 % under vacuum. Then, the pellets of CDs were dispersed in LLC solution. Subsequently, this solution was coated over silver thin films by spin coater. Hence, a gel was formed in which the carbon dots were embedded. Afterward, coated silver thin films were put on the glass prism made of BK7 which contained index matching

fluid. Index matching fluids reduce unwanted optical reflections. Surface plasmons of silver thin films were excited by utilizing glass prism made of BK7 and a tunable laser light source, which was supercontinuum laser (Koheras-SuperK Versa) with a spectral width of around 1 nm. Thus, excitons of CDs and propagating SPPs of Ag thin film are coupled.

2.2. Characterization Techniques

In this subsection of the thesis study, information about characterization techniques utilized is given.

2.2.1. UV-VIS Spectroscopy

UV-VIS spectroscopy is a non-destructive and quantitative characterization technique in which how much of the light passing through the sample absorbed or transmitted is measured with respect to a reference or blank. Light is sent by a light source and then passes through the sample. Afterwards, the light passes through the sample and absorbed or transmitted light is converted into an electronic signal.

In this work, absorption measurements of the solutions were conducted in a 1 cm quartz cuvette by utilizing fiber-coupled Ocean Optics spectrometer (USB4000, Ocean Optics) and balanced deuterium–tungsten halogen light source (DH2000-BAL, Ocean Optics) under ambient conditions. The detector of the spectrometer is a linear silicon CCD array. With this spectrometer, absorption measurement between 200 and 1100 nm range can be measured. Absorption data were analyzed by using a software program called OceanView from Ocean Optics, Inc.

2.2.3. Polarized Light Microscopy

A polarized light microscope is an optical microscope that contains polarizing filters, lenses and a detector. This microscope serves to characterize birefringent samples. Polarization is selected by using the first filter while polarization is selected by the second

filter once again. When these two filters are positioned perpendicular, waves cannot pass through. Birefringent samples are placed along the light beam and light is split into two waves by polarization. The waves whose polarization is affected by the sample can pass through the second filter.

In this work, LLC thin films were characterized by using polarizing light microscope. The images were achieved in the transmission mode.

2.2.4. Fluorescence Spectroscopy

Fluorescence is a type of photoluminescence (PL), which is caused by the absorption of photons. When fluorescent material is irradiated by photons, electrons of that fluorescent material get excited and go to one of the vibrational levels of the excited state. Afterward, excited electrons rotate or vibrate down to the closest excited electronic level, which is called internal conversion (non-radiative process). The electrons in that excited electronic level have some potential energy. Thus, electrons want to go back to their ground state by radiative relaxation. So, the electrons in the excited electronic level turn back to the ground state by giving their energy as a photon. This photon will be in the emission spectrum of the fluorescent material. In a typical measurement, light is produced by the light source. Then, the desired excitation wavelength is selected by using either a monochromator or filter. It follows the irradiation of the sample by the selected wavelength. After that photon is emitted in all directions. Then, some of these photons go through the second monochromator or filter. In the end, this photon is detected. The location of the detector is perpendicular to the excitation beam in order to reduce the possibility of detection of reflected or transmitted light produced from the light source.

Fluorescence lifetime (FLT) is the time that refers to how long the electrons of fluorescent material stay in the excited state before going back to their ground level. In order to measure FLT, two methods are used; one is the time-domain other one is the frequency domain. In the time-domain method, the fluorescent material is excited by using a pulsed laser. Then, the emission intensity of that sample is measured with respect to time and a decay curve is constructed. By using the slope of the decay curve, FLT is calculated. Among LFT measuring methods, time-correlated single-photon counting (TCSPC) is very useful owing to the ease of data collection and enlarged photon counting.

The ratio of photons that are emitted from the fluorescent material by radiative decay to photons absorbed by the fluorescent material is called absolute fluorescence quantum yield. To measure quantum yield, an integrating sphere (accessory for spectrofluorometers) or reference dye can be utilized.

In this work, FS5 Spectrofluorometer (Edinburgh Instruments, UK) was used to measure photoluminescence (PL), time-resolved lifetime (LT), and PLQY. Xenon lamp was utilized for PL and QY measurements. For FLT measurement, a 350 nm pulsed laser with the pulse width of 100 ps and a repetition rate of 1 MHz was used.

2.2.5. Scanning Transmission Electron Microscopy (STEM)

Scanning transmission electron microscopy (STEM), which is the combination of scanning electron microscopy and transmission electron microscopy, is a very useful technique that can be used in both transmission electron microscope and scanning electron microscope. There is no need for an additional new instrument for this technique. In SEM, electrons are sent on the sample surface and scan the surface of the sample. These electrons interact with the atoms in the sample. Upon this interaction, secondary electrons (electrons experienced elastic scattering) and backscattered electrons (electrons experienced inelastic scattering) are generated. These electrons are used to produce image. In STEM, beam of electrons scans the surface of the sample as same as in SEM. However, in STEM, transmitted electrons are used as to produce image and these transmitted electrons are detected by a high angle annular dark field (HAADF) detector.In this work, SEM (Quanta 250, FEI, Hillsboro, OR, USA) was used in scanning transmission electron microscope mode.

2.2.6. High Resolution Transmission Electron Microscopy (HRTEM)

High-resolution transmission electron microscopy (HRTEM) is a type of transmission electron microscopy (TEM) imaging. The only difference between the two is the magnification used. With these higher magnifications, visualization of lattice spacing of materials can be achieved. Thus, this technique is very vital for the morphological characterization of nanostructured materials. In HRTEM, electrons are sent

on the sample surface and transmitted through the sample on the grid to study the interaction between electrons and atoms in the sample. When electrons are transmitted through the sample, they interact with atoms of the sample either inelastic or elastic scattering. Electrons that have experienced elastic scattering conserve their energy and thus, these electrons are used to produce high-resolution images.

In this work for morphological characterization, FEI 120 kV Jeol HRTEM was used. The samples were dropped on the 200 mesh formvar/ carbon coated copper grids.

2.2.7. Fourier-Transform Infrared Spectroscopy (FT-IR)

IR spectroscopy studies the interaction of infrared light with matter. First of all, infrared light is produced from the light source. Then, IR light is directed to the sample. Some light is reflected whereas some light is absorbed or transmitted by the sample. When infrared light passes through the sample, vibrations of molecular bonds are triggered. The transmitted light reaches the detector to create electronic signal. This electronic signal is converted into spectrum by applying Fourier transforming.

In this work, the PerkinElmer Spectrum 65 FT-IR Spectrometer and as sampling technique attenuated total reflection (ATR) accessory were used.

CHAPTER 3

RESULTS AND DISCUSSION

3.1. Colloidal Nanodisk Shaped Plexcitonic Nanoparticles

Wet chemical synthesis of silver nanoprisms (Ag NPs) in aqueous environment was achieved via seed mediated growth, as previously described.[84,85] Seed mediated growth of silver nanoprisms consists of two steps; the procedure is depicted schematically in Figure 3.1.
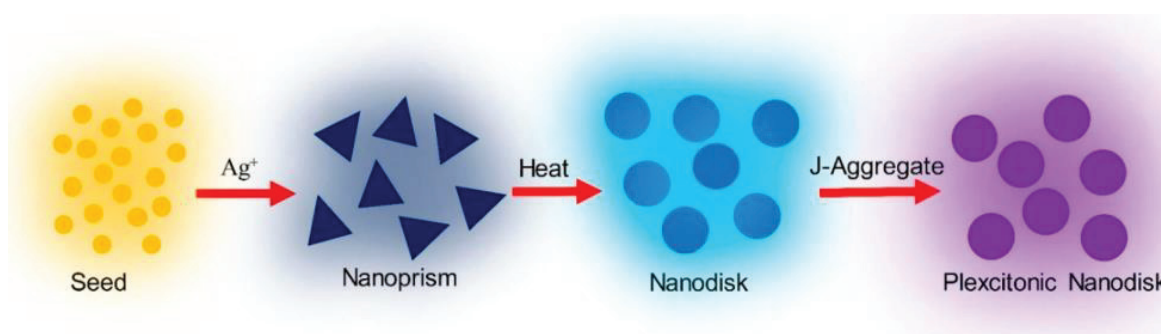
Figure 3.1. Schematic representation of the shape evolution of plasmonic nanoparticles and synthesis of plexcitonic nanodisks.[11] Reprinted with permission from Balci, F. M.; Sarisozen, S.; Polat, N.; Balci, S. Colloidal Nanodisk Shaped Plexcitonic Nanoparticles with Large Rabi Splitting Energies. Journal of Physical Chemistry C 2019, 123 (43). https://doi.org/10.1021/acs.jpcc.9b08834. Copyright 2019 American Chemical Society.

The synthesis of spherical and isotropic Ag nanoparticles was achieved by reducing silver ions in the presence of strong reducing agent, in our case sodium borohydride. The color of the obtained colloidal solution was yellow, which demonstrates that nanoparticles were formed. The plasmon resonance wavelength of this yellow solution, which was used as the seed to synthesize the Ag nanoprisms, is about 400 nm as shown in figure 3.2. Since the plasmon resonance wavelength of Ag nanoparticles is responsive to size, shape, and

dielectric environment, it can be tuned in the visible range of the electromagnetic spectrum by making changes in these parameters.[89,90]
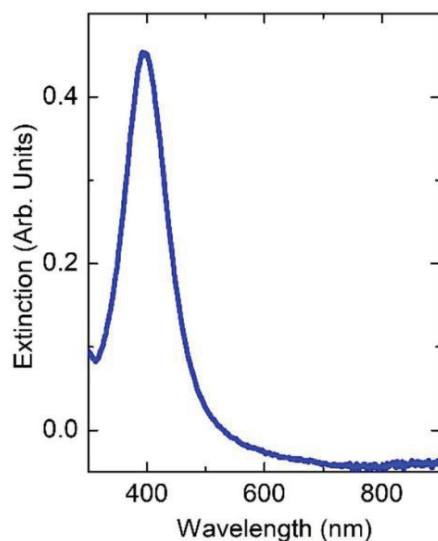
Figure 3.2. Extinction spectrum of seed silver nanoparticle colloid. Reprinted with permission from Balci, F. M.; Sarisozen, S.; Polat, N.; Balci, S. Colloidal Nanodisk Shaped Plexcitonic Nanoparticles with Large Rabi Splitting Energies. Journal of Physical Chemistry C 2019, 123 (43). https://doi.org/10.1021/acs.jpcc.9b08834. Copyright 2019 American Chemical Society.

Seed-mediated synthesis of Ag nanoprisms was conducted by reduction of silver ions by with using a weak reducing agent, in our case ascorbic acid. The size of the silver nanoprisms that were formed change according to the number of seed nanoparticles added to the reaction medium, thus the plasmon resonance wavelength of Ag nanoprisms changes in the visible range of the electromagnetic spectrum.[84] When the number of seed nanoparticles in the growth solution is high, Ag nanoprisms with short edge lengths are formed, but if small number of seed nanoparticles exists, it causes the formation of long-edged Ag nanoprisms. Since the change in size affects the location of the plasmon resonance wavelength, the plasmon resonance wavelength of the growth solution can be easily adjusted by varying the number of seed nanoparticles.

The synthesized Ag nanoprisms were converted to Ag nanodisks under the influence of heat, as shown in figure 3.3a. To manipulate the shape of Ag nanoparticles, many shape conversion methods are located in the literature. Despite the fact that initially shape transformation studies focused on obtaining Ag nanoprisms from spherical Ag

nanoparticles,[91] now it is generally focused on the transformation from nanoprisms to nanodiscs.[92] Recent studies have come to the following conclusions: (i) nanoprisms were transformed into nanodisks;[92] (ii) under the influence of heat localized plasmon resonance frequency of nanoparticles was adjusted;[93] (iii) plasmon resonance wavelength of the nanoparticles shifted to lower wavelengths (blue-shift) under heating condition;[94] (iv) it was found out that nanoprisms are not as stable as nanodiscs; [94] (v) single crystal structure is possessed by both nanoprisms and nanodisks; [92] and (vi) nanoprisms were reversibly transformed to nanodisks.[92] In another study, by performing chemical functionalization with thiol terminated poly(ethylene glycol), nanoprisms were transformed into nanodisk.[95]

This work demonstrates the formation of Ag nanodisks from Ag nanoprisms by applying heat in an oil bath at 95 °C. Time-dependent extinction spectra of one of the Ag nanoprisms heated at 95 °C in oil bath for 90 minutes is shown in figure 3.3a. The silver nanoprism, which has localized plasmon resonance at about 750 nm, shifts its localized plasmon resonance to about 550 nm under the influence of heat as shown in figure 3.3a. Figures 3.3c and 3.3d display STEM images of plasmonic particles. It is clear that the shape of the silver nanoparticles shown in Figure 3.3c is a nanoprisms. On the other hand, figure 3d shows the transformation of Ag nanoprisms into Ag nanodisks with the effect of heat. As shown in Figure 3.4, after shape transformation by applying heat, the resulting Ag nanoparticles are mostly in nanodisk morphology.

While the Ag nanoprisms are heated, they are truncated and this truncation causes the generation of nanodisk shape as shown in figure 3.5a. There are extensive studies in the literature on the synthesis of Ag nanodisks from Ag nanoprisms. The shape conversion mechanism from nanoprism to nanodisk is considered to be as follows: while the Ag nanoprisms are heated, the silver atoms, which locate on the corners of the Ag nanoprisms, dissolve and then adsorp on the side surface of Ag nanoprisms again.[86]To be able to fabricate nanodisk shaped plexcitonic nanoparticles, a cyanine dye called TDBC, which is exciton source, was utilized. TDBC is a J-aggregate dye that has the ability to self-assemble at high concentrations in the aqueous environment. The absorption band of TDBC shifts to longer wavelengths by aggregation of the molecules and is also narrowed in water. Figure 3.5b represents the absorption spectrum of TDBC in water. It is clear that TDBC has very sharp absorption peak around 587 nm. Different amounts of 0.1 mM TDBC solution were introduced to Ag nanodisk solution under stirring. Upon addition of 0.1 mM TDBC, dye molecules self-assemble on the surface of the Ag nanodisks and form organic molecular layer. The interaction between this organic molecular layer and Ag

nanodisk yields metal-organic nanoparticles. In other words, the interaction between localized surface plasmon polariton of Ag nanodisk and excitons of TDBC molecules results in strongly coupled hybrid systems which have different energy than that of both constituents.
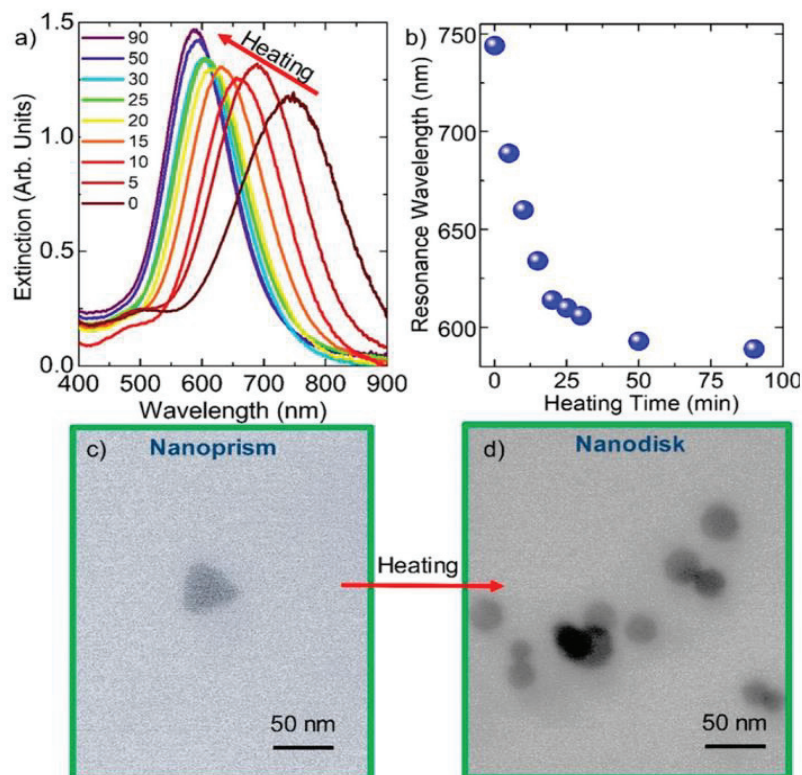
Figure 3.3. a) Transformation of extinction spectra of Ag nanoprism to Ag nanodisks under the heating condition in the time interval of 0−90 min. Ag nanoprisms having plasmon resonance wavelength approximately at 750 nm were transformed into Ag nanodisks at lower wavelengths. The direction of shifting of localized plasmon resonance wavelength is represented by the red arrow. (b) Plasmon resonance wavelength as a function of time. (c) STEM image of initial Ag nanoprisms. (d) STEM image of Ag nanodisks.[11] Reprinted with permission from Balci, F. M.; Sarisozen, S.; Polat, N.; Balci, S. Colloidal Nanodisk Shaped Plexcitonic Nanoparticles with Large Rabi Splitting Energies. Journal of Physical Chemistry C 2019, 123 (43). https://doi.org/10.1021/acs.jpcc.9b08834. Copyright 2019 American Chemical Society.

When Ag nanodisks meet with the excitonic source in this case TDBC, their resonance overlap, thus leading to the splitting of the original absorption band of the Ag nanodisk as shown in figure 3.5c. This splitting of the original absorption band of the Ag

nanodisk is a strong indication of the formation of plexcitonic nanoparticles. This separation between upper and lower branches is known as vacuum Rabi splitting.[76]
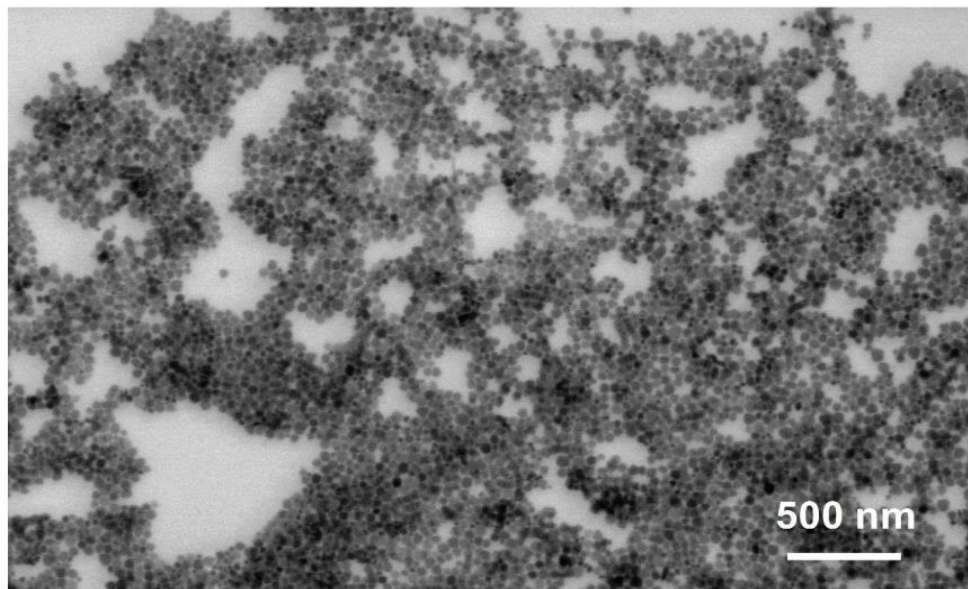
Figure 3.4. STEM image of silver nanoparticles synthesized by applying heat and mostly in the morphology of nanodisk.[11] Reprinted with permission from Balci, F. M.; Sarisozen, S.; Polat, N.; Balci, S. Colloidal Nanodisk Shaped Plexcitonic Nanoparticles with Large Rabi Splitting Energies. Journal of Physical Chemistry C 2019, 123 (43). https://doi.org/10.1021/acs.jpcc.9b08834. Copyright 2019 American Chemical Society.

The Rabi splitting energy yields information about the coupling strength and the amount of energy exchanged between plasmon and exciton.[10] In addition, the color of the solution of plexcitonic nanoparticles is different than that of the color of the solution of Ag nanodisk, see Figures 3.5a and 3.5c. In order to get rid of excess dye molecules in the solution, nanodisk shaped plexcitonic nanoparticles were centrifuged. The supernatants were removed and the pellets were redispersed in water. Thus, the resulting solution does not contain any excess dye molecules and only includes nanodisk shaped plexcitonic nanoparticles. Furthermore, the number of dye molecules conjoined to Ag nanodisks can be adjusted by adding different amounts of dye molecules to the reaction media (Figure 3.6).

31
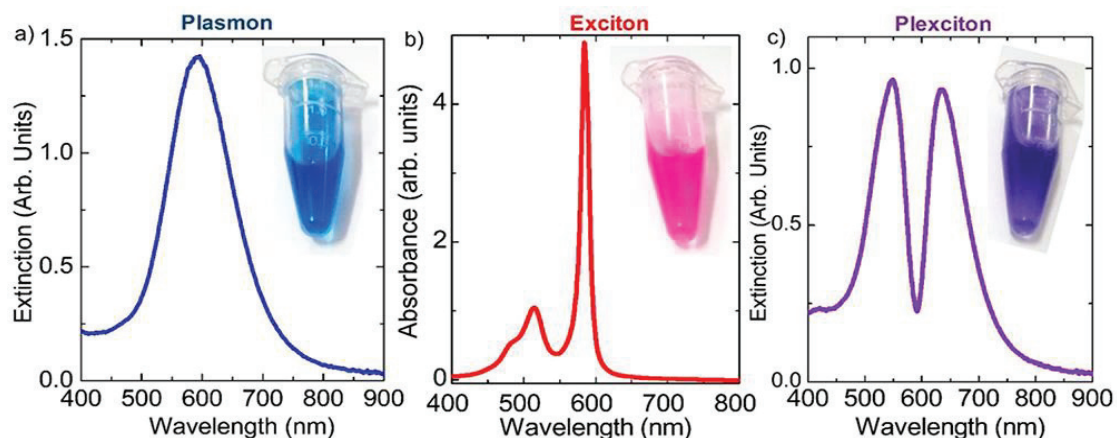
Figure 3.5. a) Extinction spectrum of Ag nanodisk in aqueous environment. b) Absorption spectrum of TDBC dye aqueous environment. c) Extinction spectrum of disk shaped plexcitonic nanoparticle in aqueous environment.[11] Reprinted with permission from Balci, F. M.; Sarisozen, S.; Polat, N.; Balci, S. Colloidal Nanodisk Shaped Plexcitonic Nanoparticles with Large Rabi Splitting Energies. Journal of Physical Chemistry C 2019, 123 (43). https://doi.org/10.1021/acs.jpcc.9b08834. Copyright 2019 American Chemical Society.

The color change with increasing dye concentration on the surface of the Ag nanodisk is shown in the photograph in Figure 3.6a. The dye concentration starts to increase as go from left to right in the photograph. Figure 3.6b displays the extinction spectra of both the Ag nanodisk and nanodisk shaped plexcitonic nanoparticles with different Rabi splitting energies. For the exciton and plasmon to interact strongly, the energy transfer rate between them, g, is greater than the plasmon decay rate (κ) and the exciton decay rate (γ) ($g \gg \gamma, \kappa$).[96] In such strongly coupled systems, there is a reversible energy flow between plasmon and exciton.[97] On the other hand, for the exciton and plasmon to interact weakly, the energy transfer rate between them, g, is smaller than both the plasmon decay rate (κ) and the exciton decay rate (γ) ($g \ll \gamma, \kappa$).[98] Figure 3.6b shows the transformation from the weakly coupled system to a strongly coupled system by increasing the dye concentration in the reaction media. The red arrow in Figure 3.6b represents the increase in dye concentration. It is undeniable that the magnitude of the Rabi splitting energy, which assigns the strength of plasmon-exciton coupling, can be varied with changing the dye concentration.[97] As the number of dye molecules increases in the Ag nanodisk colloid, the magnitude of Rabi splitting energy enhances until it gets at saturation see in figure 3.6b.
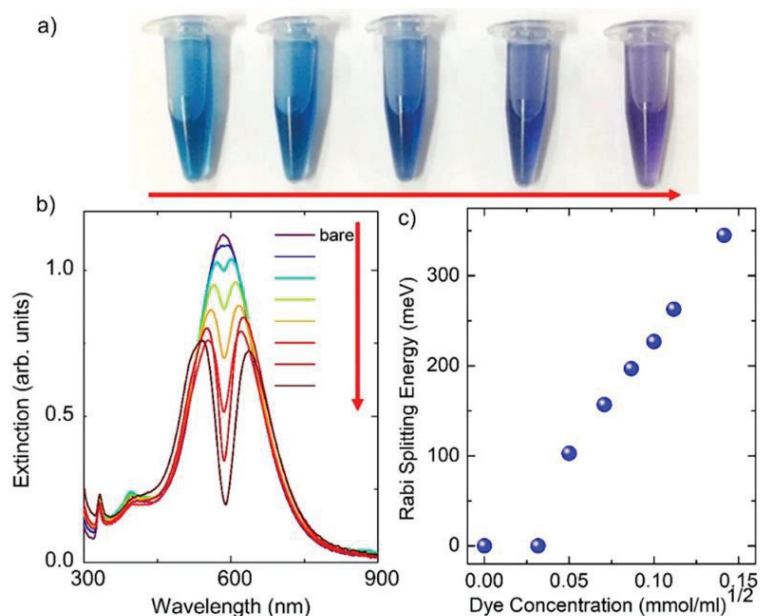
Figure 3.6. (a) A photo of Ag nanodisks containing different amounts of 0.1mM TDBC. (b) Extinction spectra of Ag nanodisks containing different amounts of 0.1 mM TDBC. (c) Rabi splitting energies obtained by utilizing data from figure b.[11] Reprinted with permission from Balci, F. M.; Sarisozen, S.; Polat, N.; Balci, S. Colloidal Nanodisk Shaped Plexcitonic Nanoparticles with Large Rabi Splitting Energies. Journal of Physical Chemistry C 2019, 123 (43). https://doi.org/10.1021/acs.jpcc.9b08834. Copyright 2019 American Chemical Society.

3.2. Decahedral Shaped Ag Nanocrystals and Strong Light- Matter Coupling in Decahedral Ag-Au Alloyed Nanocrystals

The photochemical production of decahedral shaped Ag nanoparticles from spherical Ag nanoparticles is depicted schematically in Fig. 3.7. Figure 3.8b shows the extinction spectra of spherical, isotropic Ag nanoparticles in water. The solution of spherical, isotropic Ag nanoparticles is yellow in color and possesses localized surface plasmon polariton wavelength at about 400 nm as shown in figure 3.7.
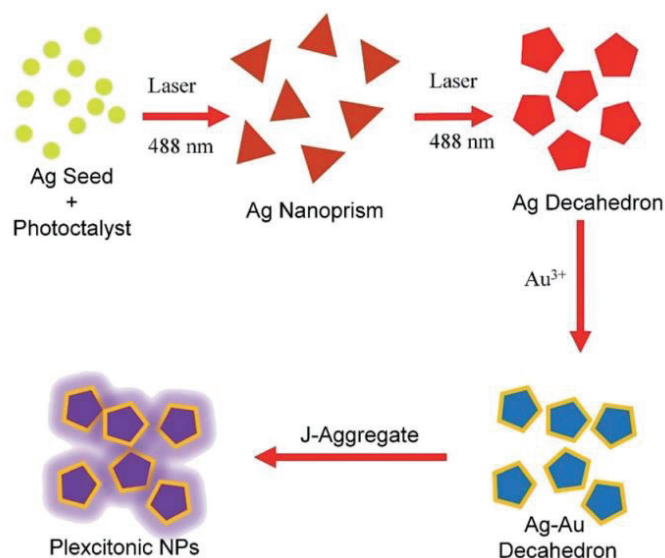
Figure 3.7. Photochemical synthesis of decahedral shaped Ag nanoparticles.[12] Reprinted with permission from Balci, F. M.; Sarisozen, S.; Polat, N.; Guvenc, C. M.; Karadeniz, U.; Tertemiz, A.; Balci, S. Laser Assisted Synthesis of Anisotropic Metal Nanocrystals and Strong Light-Matter Coupling in Decahedral Bimetallic Nanocrystals. Nanoscale Advances 2021, 3 (6) https://doi.org/10.1039/d0na00829j. Copyright 2021 Royal Society of Chemistry.

The plasmon resonance wavelength of isotropic Ag nanoparticles can be efficiently adjusted over the whole visible and near-infrared region of the electromagnetic spectrum by changing the form of the nanoparticles. L-arginine, which is one of the amino acids utilized in the biosynthesis of proteins, was utilized as a photocatalyst for the synthesis of decahedral Ag nanoparticles.[87] Unlike other studies, in this study, instead of using blue LED or white light as a light source, a blue laser at 488 nm was utilized. As shown in figure 3.8a, chemically produced isotropic spherical Ag nanoparticles were illuminated by a 488 nm laser at room temperature and pressure for the synthesis of decahedral shaped Ag nanoparticles. Lasers have previously been utilized to produce monometallic and bimetallic isotropic nanoparticles.[99,100] In contrast to earlier studies in the literature, we have come to the following conclusions as a result of these studies: (i) synthesis of decahedral Ag nanoparticles by blue laser at 488 nm, (ii) separation of Ag nanoprism and Ag decahedral nanoparticles by centrifugation, (iii) production of Ag-Au bimetallic decahedral shaped nanoparticles by galvanic replacement reaction, (iv) synthesis of plexcitonic nanoparticles from silver-gold bimetallic decahedral shaped nanoparticles, (v)

34

achieving plasmon-plasmon coupling between silver-gold bimetallic decahedral shaped nanoparticles and flat Ag thin film by Kretschmann configuration. Moreover, to be able to confirm that experimental results match the theoretical calculation, plasmonic nanoparticles, plexcitonic nanoparticles, and plasmon-plasmon hybridization in decahedral nanoparticles on flat Ag films were FDTD simulated. After exposing spherical silver nanoparticles to the blue laser at 488 nm, it was observed that the resulting anisotropic solution has its localized surface plasmon polariton resonance wavelength at about 490 nm as shown in extinction spectra in figure 3.8b.
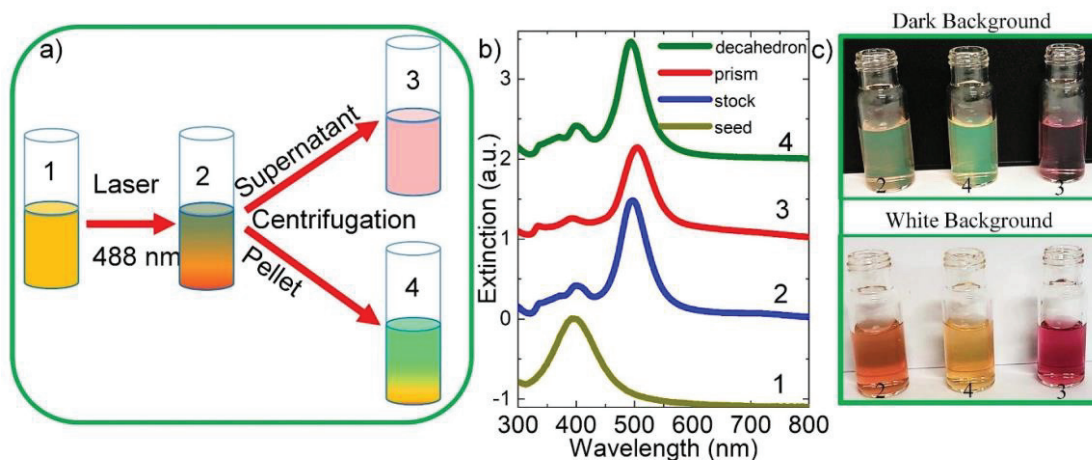
Figure 3.8. a) Synthesis of decahedral Ag nanoparticles and nanoprisms by blue laser at 488 nm and separation of Ag nanoprism and Ag decahedral nanoparticles by centrifugation. b) Extinction spectra of Ag nanoprisms, decahedral and spherical Ag nanoparticles. c) Photos of anisotropic Ag colloid, decahedral Ag nanoparticle and Ag nanoprisms .[12] Reprinted with permission from Balci, F. M.; Sarisozen, S.; Polat, N.; Guvenc, C. M.; Karadeniz, U.; Tertemiz, A.; Balci, S. Laser Assisted Synthesis of Anisotropic Metal Nanocrystals and Strong Light-Matter Coupling in Decahedral Bimetallic Nanocrystals. Nanoscale Advances 2021, 3 (6) https://doi.org/10.1039/d0na00829j. Copyright 2021 Royal Society of Chemistry.

There are both prisms and decahedra in the colloid solution formed after about 15 hours. The low-intensity peak at about 400 nm indicates that spherical Ag nanoparticles, which is used as seed, are still present in the colloid. We discovered that irradiating the spherical Ag nanoparticles for 15 hours is adequate to transform almost all of the spherical Ag nanoparticles into anisotropic Ag nanoparticles by measuring the absorbance as a function of exposure duration.

Through centrifugation, Ag nanoprisms and decahedral Ag nanoparticles were separated from each other as shown in figure 3.8a. Figure 3.8c shows that decahedral Ag nanoparticles are bicolored, whereas Ag nanoprism is monocolored. STEM image of decahedral Ag nanoparticles is represented in figure 3.9.
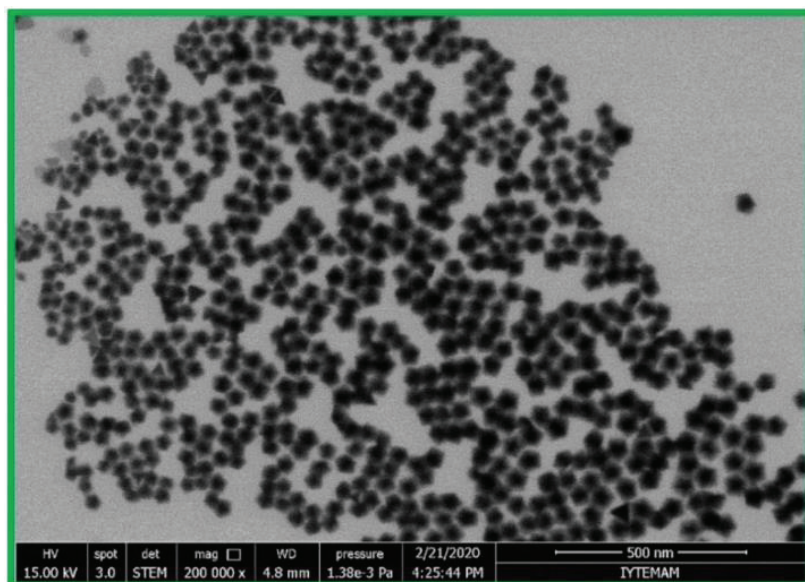
Figure 3.9. STEM image of laser assisted synthesized decahedral Ag nanoparticles.12 Reprinted with permission from Balci, F. M.; Sarisozen, S.; Polat, N.; Guvenc, C. M.; Karadeniz, U.; Tertemiz, A.; Balci, S. Laser Assisted Synthesis of Anisotropic Metal Nanocrystals and Strong Light-Matter Coupling in Decahedral Bimetallic Nanocrystals. Nanoscale Advances 2021, 3 (6) https://doi.org/10.1039/d0na00829j. Copyright 2021 Royal Society of Chemistry.

It can be clearly seen from STEM image that the Ag nanoparticles are in decahedral shape. Besides, the average size of decahedral Ag nanoparticles is about 50 nm. As shown in figure 3.10, the plasmon resonance wavelength of decahedral shaped Ag nanoparticles can be tuned via galvanic replacement reaction Ag and Au3+. Thus, bimetallic decahedral shaped nanoparticles were generated. In 2008, Pietrobon et. al[87] obtained decahedral shaped Ag nanoparticles with adjustable plasmon resonances by introducing spherical Ag nanoparticles to decahedral shaped Ag nanoparticle solution during irradiation by visible light.

Galvanic replacement reaction is very attractive method to prepare bimetallic nanoparticles, because it occurs when metals with different standard electrochemical reduction potentials meet. The difference in electrochemical reduction potential of silver atoms and gold ions leads to oxidation of decahedral shaped Ag nanoparticles through gold ions, thus Ag-Au bimetallic decahedral shaped nanoparticles were generated.

$$Au^{3+} + 3Ag \rightarrow Au + 3Ag^+, \Delta E^o = +0.7 \text{ V} \qquad (1)$$

The Gibbs free energy of the electrochemical reaction between silver atoms and gold ions is negative due to the equation below, thus it is a spontaneous reaction.[20]

$$\Delta G^o = -nFE^o \qquad (2)$$

ΔGo is Gibbs free energy, n is the number of electrons, F is Faraday constant and Eo is the standard cell potential of the electrochemical reaction.

Photos from 1 to 6 in figure 3.10a represent decahedral shaped Ag nanoparticles that contain different concentrations of gold ions. The first (0) photo on the left in figure 4a shows how decahedral shaped Ag nanoparticles appear on a dark background whereas the second (1) photo on the left in figure 4a displays how decahedral shaped Ag nanoparticles appear on a white background. On the other hand, other photographs show Ag-Au bimetallic decahedral shaped nanoparticles with different amounts of gold added. As going from left to right, the number of gold ions, which were added to the solution Ag decahedral nanoparticle, enhances.

Figure 3.10b shows the extinction spectra of Ag decahedral shaped nanoparticles after adding different quantities of gold ions, as well as the associated localized SPP resonance shift. Localized surface plasmon polariton resonance wavelength can be tuned by introducing gold ions into Ag decahedral shaped nanoparticle colloid, subsequently, galvanic displacement reaction between silver atoms and gold ions occurs. Thus, electrochemical reaction changes the optical properties of Ag decahedral shaped nanoparticles. As a result, Ag nanoparticles' localized surface plasmon polariton resonance wavelength can be altered by more than 200 nm, as shown in Fig. 3.10c. Thanks to the addition of gold ions that cover Ag nanoparticles, the stability of Ag decahedral shaped nanoparticles has been substantially increased.
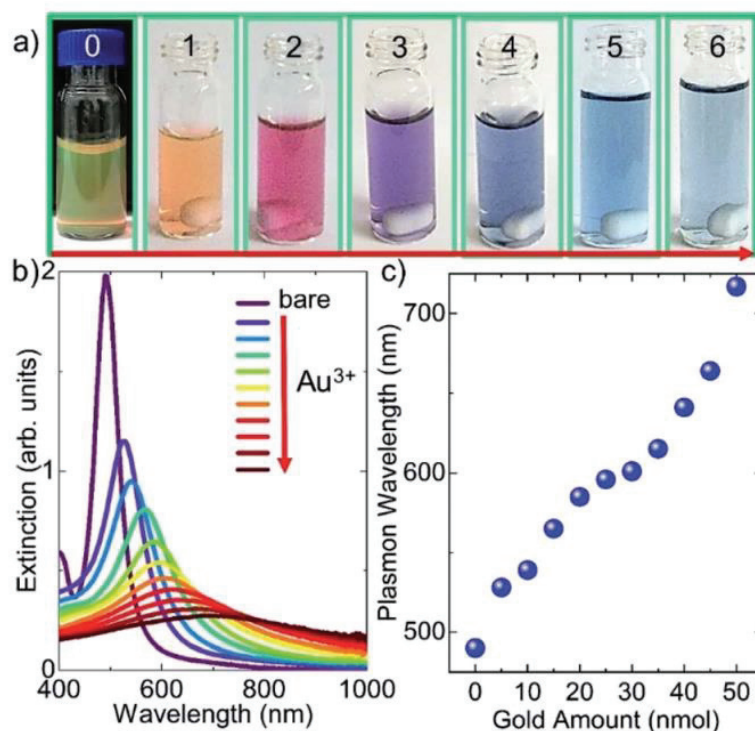
Figure 3.10. a) The first (0) and second (1) photos shows the (monometallic) Ag decahedral shaped nanoparticle solution in the dark and white background. Other photographs from 2 to 6 show Ag-Au bimetallic decahedral shaped nanoparticles with different amounts of gold added. As going from left to right the amount of gold ions in the solution increases. (b) Extinction spectra of the Ag decahedral shaped nanoparticles and Ag-Au bimetallic decahedral shaped nanoparticles which contain different amounts of gold ions. As the concentration of gold ions increases in the colloid, localized surface plasmon polariton resonance wavelength shifts to longer wavelengths owing to galvanic replacement reaction between silver atoms and gold ions. (c) Change in the plasmon polariton resonance wavelength with respect to gold amount.[12] Reprinted with permission from Balci, F. M.; Sarisozen, S.; Polat, N.; Guvenc, C. M.; Karadeniz, U.; Tertemiz, A.; Balci, S. Laser Assisted Synthesis of Anisotropic Metal Nanocrystals and Strong Light-Matter Coupling in Decahedral Bimetallic Nanocrystals. Nanoscale Advances 2021, 3 (6) https://doi.org/10.1039/d0na00829j. Copyright 2021 Royal Society of Chemistry.

A single gold ion displaces three silver atoms throughout the galvanic replacement reaction. Therefore, as observed in our prior research,[20] tiny gaps in gold-covered Ag nanoparticles may exist. Indeed, STEM images of Ag-Au bimetallic decahedral shaped nanoparticles prove that the form of nanoparticles is retained upon the addition of gold ions, see in figure 3.11. Besides, energy dispersive X-ray (EDX) elemental analysis reveals that Ag-Au bimetallic decahedral shaped nanoparticles were formed, as shown in figure 3.12.
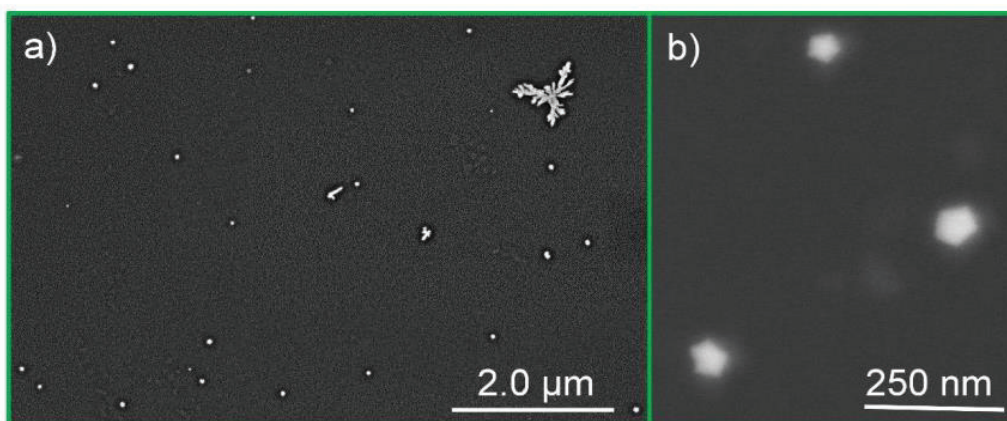
Figure 3.11. a) Large area STEM image of Ag-Au bimetallic decahedral shaped nanoparticles. b) Small area STEM image of Ag-Au bimetallic decahedral shaped nanoparticles. [12]Reprinted with permission from Balci, F. M.; Sarisozen, S.; Polat, N.; Guvenc, C. M.; Karadeniz, U.; Tertemiz, A.; Balci, S. Laser Assisted Synthesis of Anisotropic Metal Nanocrystals and Strong Light-Matter Coupling in Decahedral Bimetallic Nanocrystals. Nanoscale Advances 2021, 3 (6) https://doi.org/10.1039/d0na00829j. Copyright 2021 Royal Society of Chemistry.

To be able to fabricate Ag-Au decahedral shaped plexcitonic nanoparticles, TDBC was utilized as a J-aggregate dye. TDBC has exciton resonance wavelength of about 585 nm, as shown in figure 3.13c. The photochemically synthesized Ag decahedral shaped nanoparticles, on the other hand, exhibit a plasmon resonance wavelength of roughly 490 nm (see figure 3.13a). Galvanic replacement reaction was utilized for the synthesis of Ag-Au bimetallic decahedral shaped nanoparticles in order to achieve spectral overlap between the plasmon resonance of nanoparticle and the exciton transition in J-aggregates as shown in figure 3.13b. Note that the localized surface plasmon polariton resonance After the addition of TDBC to Ag-Au bimetallic decahedral shaped nanoparticle, the localized surface plasmon polariton resonance wavelength of the bimetallic nanoparticle split into

lower and upper branches. wavelength shifted about from 490 to 600 nm after galvanic replacement reaction as shown in figure 3.13b.

Element	Wt%	Atomic %
C	7.18	15.62
O	1.85	3.02
Na	0.45	0.51
Si	85.57	79.67
Ag	4.75	1.15
Au	0.21	0.03
Total:	100.00	100.00
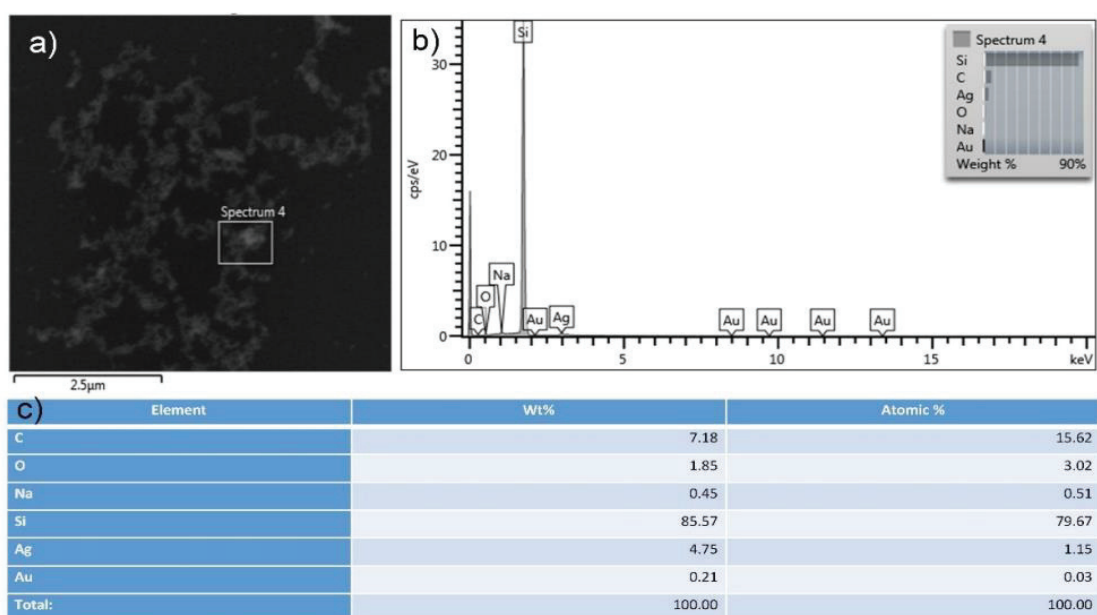
Figure 3.12. (a) Large area SEM image of the Ag-Au bimetallic decahedral shaped nanoparticles. (b) EDX spectrum of the selected area in SEM image. (c) Detected elements by the EDX analysis. The Ag-Au bimetallic decahedral shaped nanoparticles were dropped on a silicon wafer and thus silicon elements also appear in the spectrum.[12] Reprinted with permission from Balci, F. M.; Sarisozen, S.; Polat, N.; Guvenc, C. M.; Karadeniz, U.; Tertemiz, A.; Balci, S. Laser Assisted Synthesis of Anisotropic Metal Nanocrystals and Strong Light-Matter Coupling in Decahedral Bimetallic Nanocrystals. Nanoscale Advances 2021, 3 (6) https://doi.org/10.1039/d0na00829j. Copyright 2021 Royal Society of Chemistry.

This splitting proves the strong interaction between localized surface plasmon polaritons of bimetallic nanoparticles and excitons in J-aggregate dye (see figure 3.13c). Besides, the extinction spectra of Ag decahedral shaped nanoparticles, Ag-Au bimetallic decahedral shaped nanoparticles, and Ag-Au bimetallic decahedral shaped plexcitonic nanoparticles were the finite time-domain (FDTD) simulated to corroborate the experimental results with theoretical results as shown in figure 3.14. As seen in Figure 3.14, theoretical calculations and experimental data agree with each other. Sharp corners of Ag decahedral shaped nanoparticles are very conducive to enhancement in light-matter interaction. Consequently, to understand light-matter interaction at nanoscale dimensions,

Ag decahedral shaped nanoparticles can be utilized, e.g, single-molecule strong coupling at room temperature.[101]
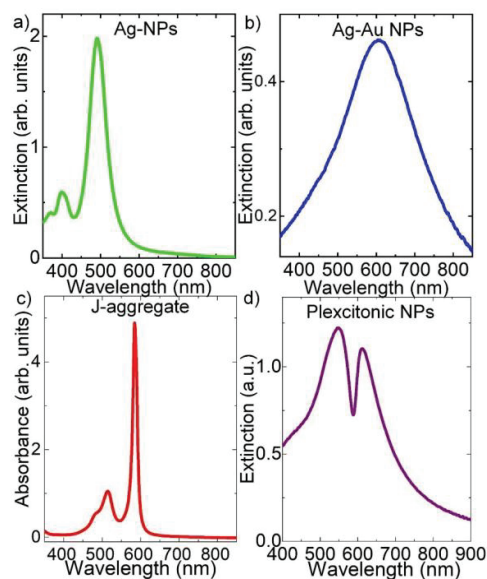
Figure 3.13. (a) Extinction spectrum of Ag decahedral shaped nanoparticles in water. (b) Extinction spectrum of Ag-Au bimetallic decahedral shaped nanoparticles in water. (c) Absorbance spectrum of J-aggregate dye, TDBC, in water. (d) Extinction spectrum of Ag-Au decahedral shaped plexcitonic nanoparticles.[12] Reprinted with permission from Balci, F. M.; Sarisozen, S.; Polat, N.; Guvenc, C. M.; Karadeniz, U.; Tertemiz, A.; Balci, S. Laser Assisted Synthesis of Anisotropic Metal Nanocrystals and Strong Light-Matter Coupling in Decahedral Bimetallic Nanocrystals. Nanoscale Advances 2021, 3 (6) https://doi.org/10.1039/d0na00829j. Copyright 2021 Royal Society of Chemistry.

Plasmon-plasmon coupling between Ag-Au bimetallic decahedral shaped nanoparticles and flat Ag thin film was studied. Both plasmon resonance shifts and massive increments in an electric field can be caused by plasmon–plasmon coupling between localized surface plasmon polaritons of metal nanoparticles and propagating surface plasmon polaritons of flat metal thin films, hence are commonly used in surface-enhanced spectroscopies, strong plasmon–exciton couplings, plasmonic light sources, and solar cells.[102,103] Plasmon-plasmon coupling between Ag-Au bimetallic decahedral shaped nanoparticles and flat Ag thin film was achieved by Kretschmann configuration.[88]
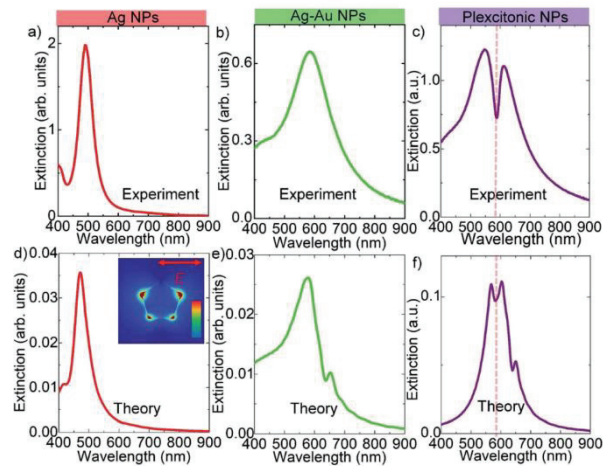
Figure 3.14. Experimental extinction spectrum of (a) Ag decahedral shaped nanoparticles, (b) Ag-Au bimetallic decahedral shaped nanoparticles, and (c) Ag-Au bimetallic decahedral shaped plexcitonic nanoparticles. Theoretical extinction spectra of (d) Ag decahedral shaped nanoparticles (e) Ag-Au bimetallic decahedral shaped nanoparticles, and (f) Ag-Au bimetallic decahedral shaped plexcitonic nanoparticles. The electric field distribution in the resonant excitation in the Ag decahedral shaped nanoparticles is shown as an inset in (d).[12] Reprinted with permission from Balci, F. M.; Sarisozen, S.; Polat, N.; Guvenc, C. M.; Karadeniz, U.; Tertemiz, A.; Balci, S. Laser Assisted Synthesis of Anisotropic Metal Nanocrystals and Strong Light-Matter Coupling in Decahedral Bimetallic Nanocrystals. Nanoscale Advances 2021, 3 (6) https://doi.org/10.1039/d0na00829j. Copyright 2021 Royal Society of Chemistry.

Surface plasmons on flat Ag thin films are often excited using the Kretschmann arrangement. The experimental setup utilized to study the interaction of localized and propagating surface plasmon polaritons is depicted schematically in figure 3.15a. To investigate the interaction between localized and propagating surface plasmon polaritons, at each angle of incidence, spectroscopic reflection measurements, which depend on polarization, were taken.

Through a tunable laser light source, which was supercontinuum laser with a spectral width of around 1 nm, and glass prism made of BK7, surface plasmons of flat Ag thin film were excited. For electrostatically self-assembly of Ag-Au bimetallic decahedral shaped nanoparticles on the surface of the flat Ag thin film, surface modification was required. To modify the surface of flat Ag thin film, self-assembled monolayer of thiols provided by 16-mercaptohexadecanoic acid was used, subsequently it followed by further

modification via self-assembled monolayers of aminosilanes provided by (3-aminopropyl)trimethoxysilane.
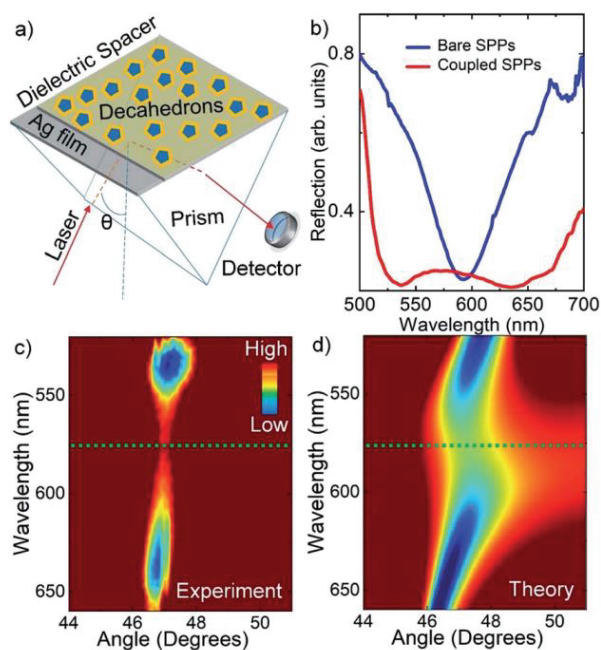
Figure 3.15. (a) The experimental setup utilized to excite surface plasmons on flat Ag thin film is depicted schematically. (b) Reflection spectra of a bare flat Ag thin film and a coupled Ag-Au bimetallic decahedral shaped nanoparticles with Ag thin film. (c) Experimentally achieved dispersion curve of Ag-Au bimetallic decahedral shaped nanoparticles on the flat Ag thin film. (d) Theoretically achieved dispersion curve of Ag-Au bimetallic decahedral nanoparticles on the flat Ag thin film.[12] Reprinted with permission from Balci, F. M.; Sarisozen, S.; Polat, N.; Guvenc, C. M.; Karadeniz, U.; Tertemiz, A.; Balci, S. Laser Assisted Synthesis of Anisotropic Metal Nanocrystals and Strong Light-Matter Coupling in Decahedral Bimetallic Nanocrystals. Nanoscale Advances 2021, 3 (6) https://doi.org/10.1039/d0na00829j. Copyright 2021 Royal Society of Chemistry.

Through surface modification, Ag-Au bimetallic decahedral shaped nanoparticles self-assembled on the chemically treated surface of the flat Ag thin film electrostatically in water.[88] Figure 3.15b displays reflection spectra of a bare flat Ag thin film and a coupled Ag-Au bimetallic decahedral shaped nanoparticles with flat Ag thin film. The localized surface plasmon polaritons of Ag-Au bimetallic decahedral shaped nanoparticles are strongly coupled to propagating surface plasmon polaritons of flat Ag thin films, as shown in the dispersion curve in figure 3.15c. The dispersion curve of bare flat Ag thin film does

not possess anticrossing behavior whereas anticrossing behavior proves that there is the strong interaction between the localized surface plasmon polaritons of Ag-Au bimetallic decahedral shaped nanoparticles and propagating surface plasmon polaritons of flat Ag thin film. In other words, localized surface plasmon polaritons of Ag-Au bimetallic decahedral shaped nanoparticles strongly coupled to propagating surface plasmon polaritons of flat Ag thin film as shown in figures 3.16c and 3.16d. To confirm the experimental results corroborate with theoretical results, the dispersion curves of bare flat Ag thin film and Ag-Au bimetallic decahedral shaped nanoparticles coated on flat Ag thin film were FDTD simulated. As can be seen in Figure 10, theoretical and experimental studies agree with each other.
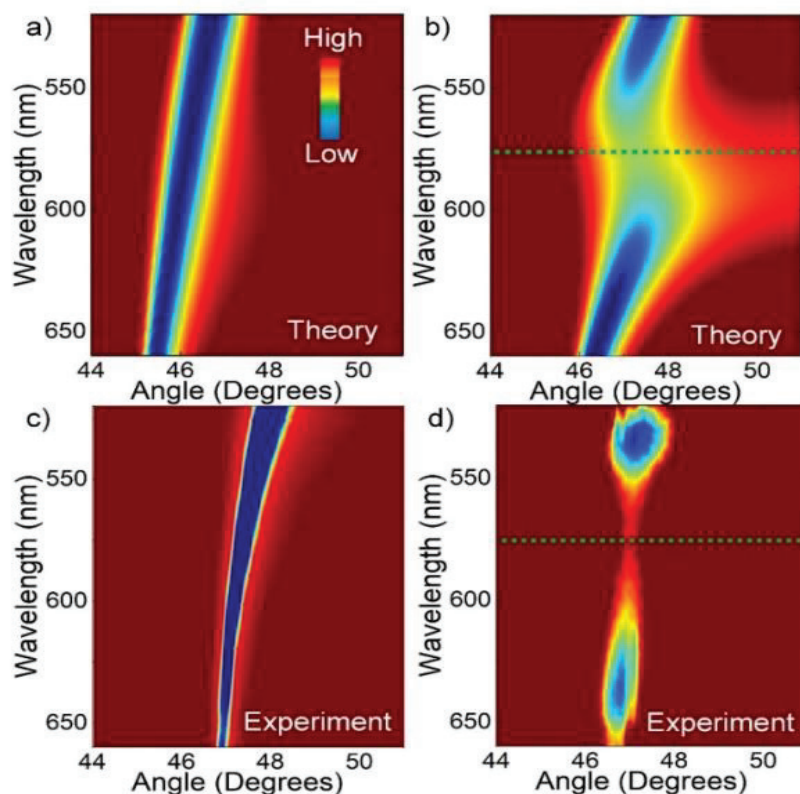
Figure 3.16. (a) Theoretical dispersion curve of bare Ag film. (b) Theoretical dispersion curve of coated Ag film coated. (c) Experimental dispersion curve of bare Ag film. (d) Experimental dispersion curve of Ag-Au bimetallic decahedral shaped nanoparticles self-assembled on Ag film.[12] Reprinted with permission from Balci, F. M.; Sarisozen, S.; Polat, N.; Guvenc, C. M.; Karadeniz, U.; Tertemiz, A.; Balci, S. Laser Assisted Synthesis of Anisotropic Metal Nanocrystals and Strong Light-Matter Coupling in Decahedral Bimetallic Nanocrystals. Nanoscale Advances 2021, 3 (6) https://doi.org/10.1039/d0na00829j. Copyright 2021 Royal Society of Chemistry.

3.3. Strong Coupling of Carbon Quantum Dots in Liquid Crystals

A hydrothermal method was used to synthesize carbon quantum dots (CDs) by utilizing L-phenylalanine (LPA) and ortho-phenylendiamine (OPD) as carbon and amine precursor at high temperature in Teflon-lined stainless-steel autoclave for 12h, as shown in figure 3.17a. After 12 hours of hydrothermal reaction, the Teflon-coated stainless-steel autoclave was removed from the oven and allowed to cool to room temperature. The solution color at the end of the reaction was observed as dark blue while the initial color of the solution was transparent. This color change from transparent to dark blue demonstrates the formation of CDs. Centrifugation and filtration were performed to get rid of large aggregates from the CDs colloid. The resulting CD colloid possesses red luminescence when irradiated by white light. In addition, there is approximately 0.8 mg of CDs per 1 mL of colloid. NaOH solution was introduced drop by drop in dark blue colored solution in order to precipitate CD under stirring. The addition of NaOH continued until pH reached 7. In order to discard the excess amount of NaOH, the neutralized solution was centrifuged three times. In each centrifugation, the supernatant was removed and the pellet was redispersed in water. After the last centrifugation, different buffer solutions at different pH values were utilized to disperse pellets of CDs for photoluminescence measurements.

It is undeniable that the fluorescence behavior of CDs is contingent on pH values as shown in figure 3.18. By utilizing photoluminescence data dependent 2D excitation-emission topographical maps of CDs were constructed (see in figure 3.18).

It's worth mentioning that CD solutions are quite a stability at room temperature. The ideal sulfuric acid to water ratio required for the synthesis was determined to be 0.25. Lyotropic liquid crystalline (LLC) mesophases were used to disperse CDs as shown in figure 3.17b. Amphiphilic molecules have the ability to self-assemble into a variety of structures in presence of a wide range of environments, e.g, water, acids, salts, etc. LLC mesophases can be obtained by dissolving amphiphilic molecules, i.e., nonionic surfactants, in the solvent, i.e., hygroscopic species such as acids and salts. Very stable LLC mesophases are formed when the sulfuric acid/ $C_{12}E_{10}$ mole ratio of the solution prepared using sulfuric acid, one of the strong acids, and 10-lauryl ether ($C_{12}E_{10}$), one of the nonionic surfactants, is between 2 and 12.[82]
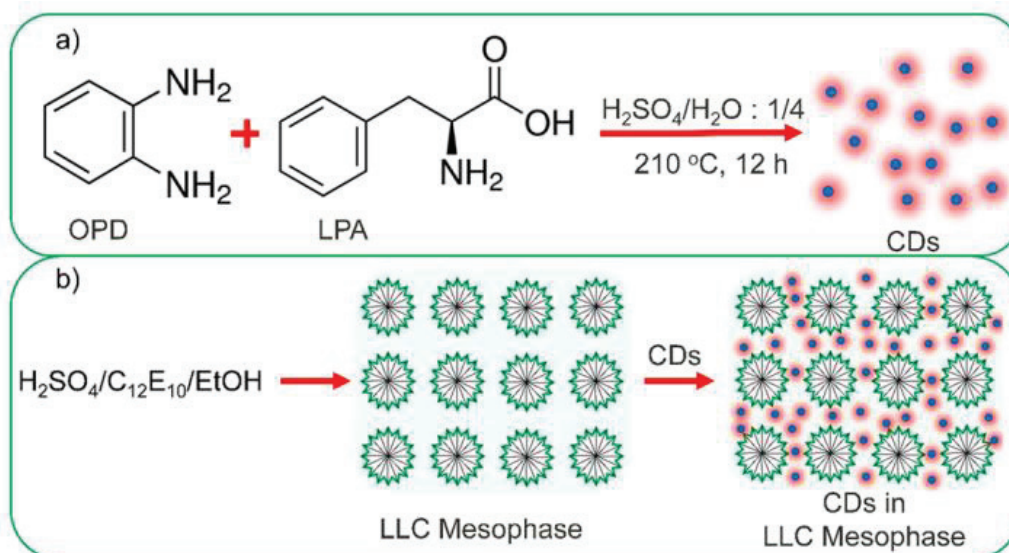
Figure 3.17. (a) Hydrothermal synthesis of red luminescent CDs (b) Preparation of LLC mesophases and confining CDs into spaces.[13] Reprinted with permission from Sarisozen, S.; Polat, N.; Mert Balci, F.; Guvenc, C. M.; Kocabas, C.; Yaglioglu, H. G.; Balci, S. Strong Coupling of Carbon Quantum Dots in Liquid Crystals. The Journal of Physical Chemistry Letters 2022, 3562–3570. https://doi.org/10.1021/acs.jpclett.1c03937. Copyright 2022 American Chemical Society.

The increase in the number of sulfuric acid results in the enhancement of the amount of water in the system. If the amount of sulfuric acid is raised from 2 to 12 per C12E10, the water absorption of the stable C12E10/sulfuric acid lyotropic liquid crystal system enhances from 2.3 to 4.3 per sulfuric acid. Two-dimensional hexagonal LLC mesophases are achieved by the combination of C12E10 and sulfuric acid with the amount of water, until the ratio of sulfuric acid to C12E10 reaches about 3.5, whereas micelle cubic LLC mesophases are formed above 3.5. A characteristic fan pattern is displayed for hexagonal LLC mesophases under a polarizing optical microscope, whereas no texture is observed for cubic LLC mesophases because it is in cubic phase refraction index is identical in every direction, hence it looks black under the polarizing optical microscope. We used a sulfuric acid/C12E10 mixture having mole ratio of 2.5 for this study; this produces a very stable hexagonal LLC mesophase with the characteristic fan texture under a polarizing optical microscope as shown in figure 3.19. Surfactant which is C12E10, sulfuric acid, and ethanol were used to form the LLC mesophases.
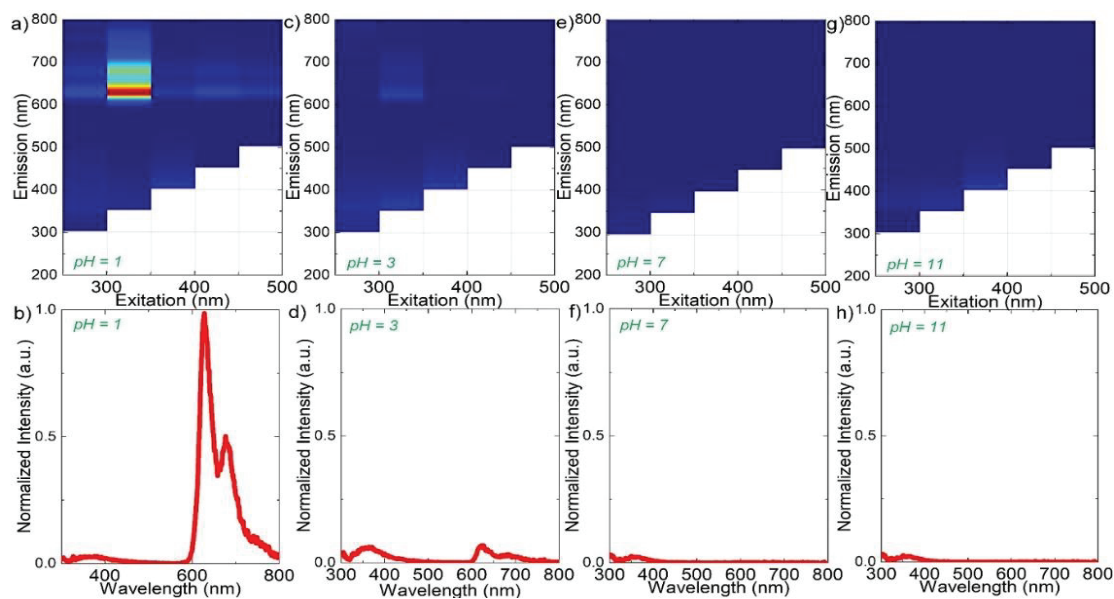
Figure 3.18. 2D excitation-emission topographical maps of CDs that are pH-dependent. (a-b) pH = 1, (c-d) pH = 3, (e-f) pH = 7, (g-h) pH = 11. The greatest PL emission intensity is shown by the red-colored region on the map, while the least PL emission intensity is indicated by the blue-colored region.[13] Reprinted with permission from Sarisozen, S.; Polat, N.; Mert Balci, F.; Guvenc, C. M.; Kocabas, C.; Yaglioglu, H. G.; Balci, S. Strong Coupling of Carbon Quantum Dots in Liquid Crystals. The Journal of Physical Chemistry Letters 2022, 3562–3570. https://doi.org/10.1021/acs.jpclett.1c03937. Copyright 2022 American Chemical Society.
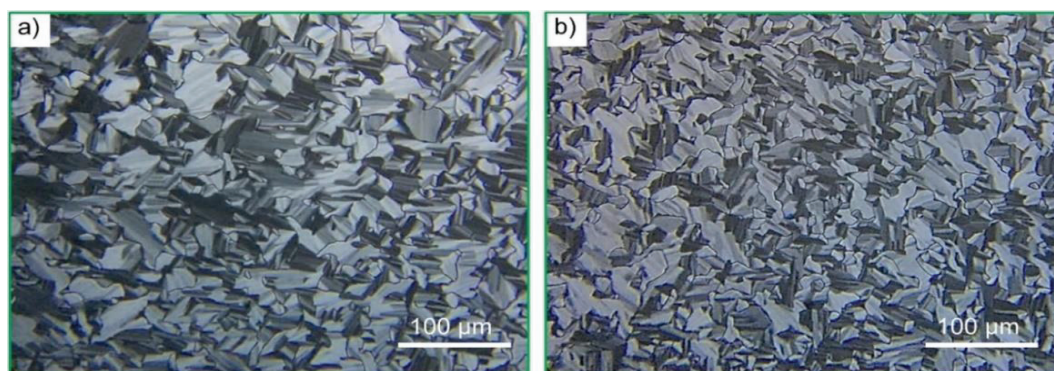
Figure 3.19. Images of (a) the hexagonal LLC mesophase and (b) the hexagonal LLC mesophase having CDs under polarizing optical microscope (POM).[13] Reprinted with permission from Sarisozen, S.; Polat, N.; Mert Balci, F.; Guvenc, C. M.; Kocabas, C.; Yaglioglu, H. G.; Balci, S. Strong Coupling of Carbon Quantum Dots in Liquid Crystals. The Journal of Physical Chemistry Letters 2022, 3562–3570. https://doi.org/10.1021/acs.jpclett.1c03937. Copyright 2022 American Chemical Society.

Red light is emitted by CDs due to the presence of sulfuric acid in the LLC mesophases. Moreover, due to embedded CDs in LLC mesophases, thin films capable of emitting red light can be formed. The mesophase is initially prepared as a solution in ethanol to be able to achieve LLC film. The red emissive gel phase is obtained as thin film by spin coating the LLC solution onto the desired substrate. It is worth noting that stable and homogeneous CD thin films could not be produced in the presence of polyvinyl alcohol (PVA) in this study; the reason for this is that the film produced with PVA may break down under a very strong acidic environment.[104]

Figure 3.20a represents the HRTEM image of the synthesized red emissive CDs while figure 3.20b shows magnified HRTEM image of single CD in the targeted area defined by the white rectangle.
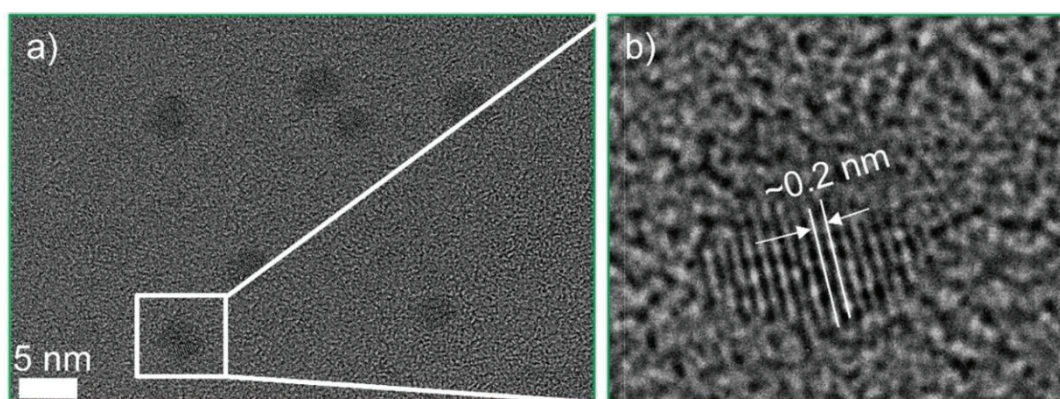
Figure 3.20. The atomic resolution of CDs is shown by TEM micrographs with high resolution (a) CDs with an average diameter of less than 5 nm as shown in a large area TEM micrograph with high resolution. (b) HRTEM image of single CD in the targeted area. A magnified HRTEM image of white marked enclosed area shown in (a) shows d spacing of roughly 0.2 nm.[13] Reprinted with permission from Sarisozen, S.; Polat, N.; Mert Balci, F.; Guvenc, C. M.; Kocabas, C.; Yaglioglu, H. G.; Balci, S. Strong Coupling of Carbon Quantum Dots in Liquid Crystals. The Journal of Physical Chemistry Letters 2022, 3562–3570. https://doi.org/10.1021/acs.jpclett.1c03937. Copyright 2022 American Chemical Society.

This high-resolution image contains lattice fringes. The crystallinity of the sample is demonstrated by the well-resolved lattice fringes. The CDs, in fact, do have high crystallinity with a lattice spacing of 0.20 nm corresponding to that of graphene (100) facet's in-plane lattice spacing.[105] As shown in figure 3.20, CDs have well-resolved lattice

fringes having a lattice spacing of roughly 0.2 nm. Defects in the crystal structure is indicated by TEM micrograph with high resolution. The average size distribution was found to be about 4 nm based on HRTEM images. Moreover, figure 3.21 shows the FTIR spectrum of the synthesized CDs, which plays vital role to determine the functional groups in the CDs. The stretching vibrations of C-OH (3300 cm^{-1}), C-H (2920 cm^{-1}), vibrational absorption of C=O (1730 cm^{-1}), and C=C (1620 cm^{-1}) are all present in the FT-IR spectrum of the CDs.[106]
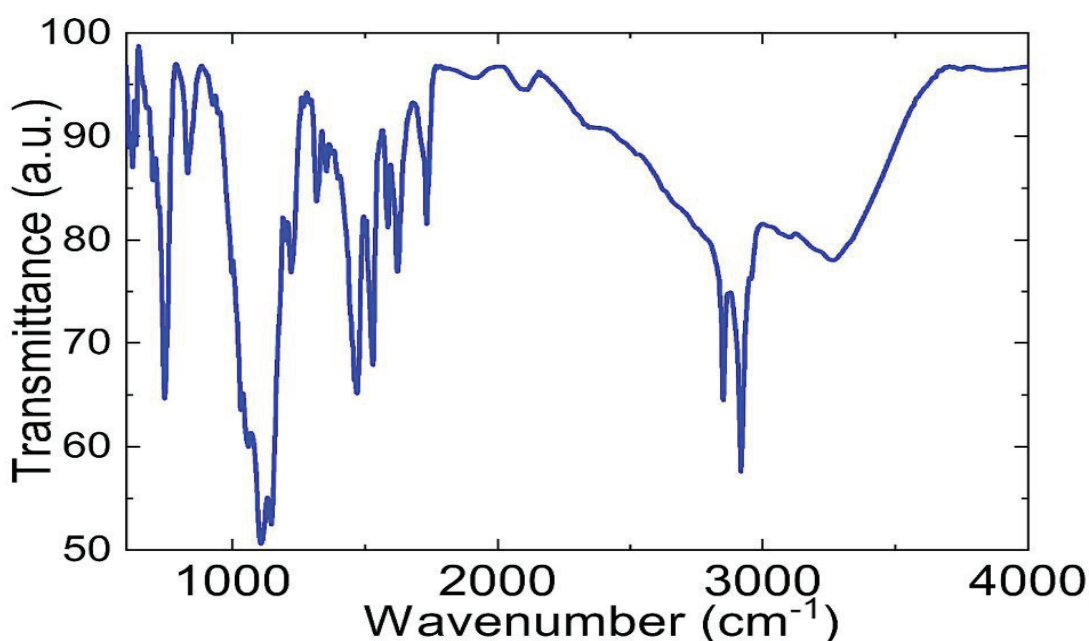
Figure 3.21. FTIR spectrum of synthesized CDs.[13] Reprinted with permission from Sarisozen, S.; Polat, N.; Mert Balci, F.; Guvenc, C. M.; Kocabas, C.; Yaglioglu, H. G.; Balci, S. Strong Coupling of Carbon Quantum Dots in Liquid Crystals. The Journal of Physical Chemistry Letters 2022, 3562–3570. https://doi.org/10.1021/acs.jpclett.1c03937. Copyright 2022 American Chemical Society.

As shown in figure 3.22, neutralized CDs were redispersed in acidic medium, and moreover, red emission was obtained when illuminated with visible light. Very sharp and strong absorption peak of the CDs is observed at 610 nm while very intense emission peak of CDs is found at around 624 nm in water see figure 6a. A UV-Vis spectrophotometer was utilized to measure the absorption spectra of CDs dispersed in various environments. The absorption peak at about 280 nm corresponds to $\pi \rightarrow \pi *$ electronic transitions of both C=N and C=C double bonds. The CDs absorb light in the lower region, which is between

500 and 650 that generating fluorescence emission both in water and ethanol. Other absorption peaks are observed in the absorption spectrum of CDs in water and the observed weak absorption peak are as follows; 560 nm, 517 nm, and 477 nm. The full width at half maximum (FWHM) of absorption and emission peaks were calculated as 22 nm and 35 nm, respectively. Taxus leaves were utilized to produce CDs by using solvothermal synthesis in prior work,[107] followed by the purification of the CDs by column chromatography. FWHM of the emission peak of the resulting purified product is extremely narrow and at around 20 nm. Triangular CDs were synthesized by solvothermal treated three-fold symmetric PG triangulogen at 200 °C with different reaction times and possess very narrow emission peaks having FWHM around 30 nm in another study.[48] In acidic aqueous solutions, the optical characteristics of CDs were examined widely at room temperature in the literature. Figure 3.19b shows the CDs' excitation-emission color map. It is clear that from figure 3.19b, when synthesized CDs were irradiated at the different excitation wavelengths, the spectral locations of the strong emission peak at approximately 624 nm and a weak emission peak at about 680 nm held their spectral location of emission wavelength. The fluorescence of synthesized CDs displays good photostability and excitation-independent emission behavior. Herein, in this study, the time-resolved single-photon counting technique was employed to determine the quantum yield (QY) of CDs in different mediums. Figure 3.23 represents the QY measurements of CDs in water and ethanol. While the QY of the synthesized carbon dots was measured as 35.4% in ethanol for red fluorescence emission, in water, however, the QY was measured as 23.4% for the strong red fluorescence emission. To conduct QY measurements, 580 nm light was used to excite CDs in acidic aqueous solution having pH of 1 whereas 570 nm light was utilized for exciting CDs in ethanol. Besides, the photoluminescence lifetime measurement of CDs was conducted in water and found as about 2 ns (see Figure 3.22c).
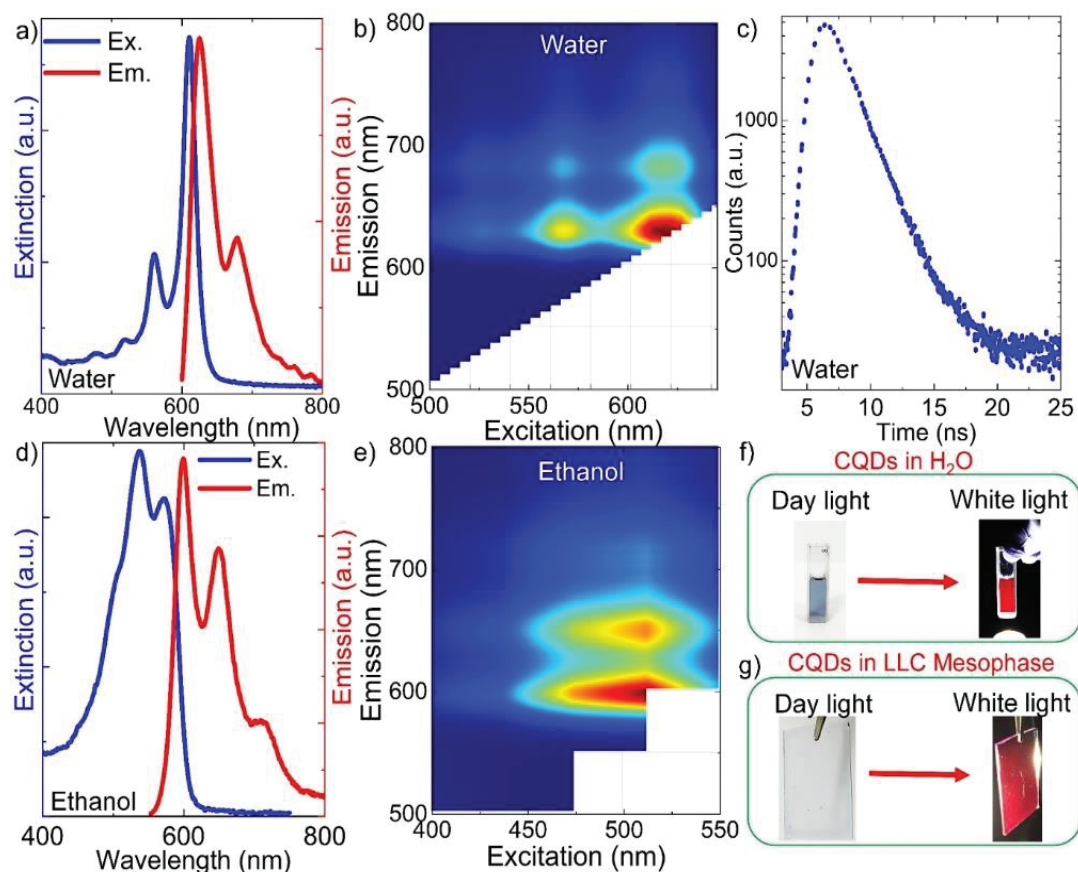
Figure 3.22. Linear optical characteristics of CDs. (a) Extinction and photoluminescence (PL) spectra of CDs measurements in water. (b) 2D excitation-emission map of CDs in water. (c) PL lifetime of CDs in water. The measured PL lifetime of CDs is about 2 ns in water. (d) Extinction and PL spectra of CDs in ethanol. (e) 2D excitation-emission map of CDs in ethanol. (f) Photo of CDs in water was left in the daylight and exposed to white light. (g) Photo of CDs dispersed in the LLC mesophase spin coated on a glass substrate was left in daylight and exposed white light. Red fluorescence emission is exhibited by both aqueous solution and LLC thin films containing CDs. [13] Reprinted with permission from Sarisozen, S.; Polat, N.; Mert Balci, F.; Guvenc, C. M.; Kocabas, C.; Yaglioglu, H. G.; Balci, S. Strong Coupling of Carbon Quantum Dots in Liquid Crystals. The Journal of Physical Chemistry Letters 2022, 3562–3570. https://doi.org/10.1021/acs.jpclett.1c03937. Copyright 2022 American Chemical Society.
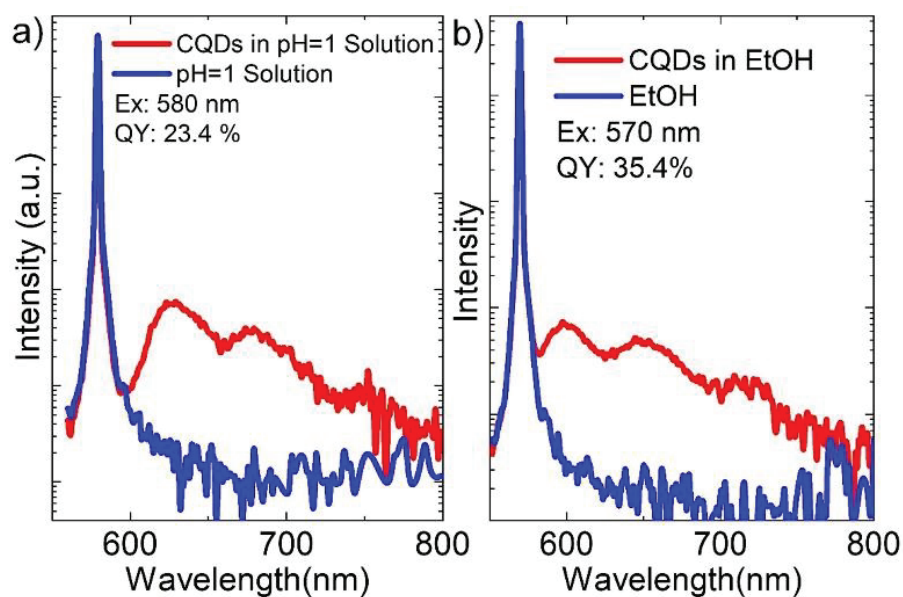
Figure 3.23. Quantum yields (QYs) of CDs were measured in (a) water as 23.4 %, and (b) ethanol as 35.4 %. [13] Reprinted with permission from Sarisozen, S.; Polat, N.; Mert Balci, F.; Guvenc, C. M.; Kocabas, C.; Yaglioglu, H. G.; Balci, S. Strong Coupling of Carbon Quantum Dots in Liquid Crystals. The Journal of Physical Chemistry Letters 2022, 3562–3570. https://doi.org/10.1021/acs.jpclett.1c03937. Copyright 2022 American Chemical Society.

The synthesized carbon dots are poorly water-soluble, which causes them to agglomerate in water, maybe this is the reason why the quantum yields may be low in water compared to ethanol. As a result, excessive energy transfer or direct π-π interactions between the CDs may lead to fluorescence emission of CDs to die down.[108]Absorption and emission spectra of CDs in ethanol are represented in figure 3.22d. Figure 3.22e shows the 2D excitation-emission color map of the CDs in ethanol. It is clear that from figure 3.22e, when synthesized CDs were irradiated at different excitation wavelengths in ethanol, the spectral location of emission wavelength did not change. The fluorescence of synthesized CDs displays excitation-independent emission behavior in ethanol. In addition, a very small and broad shoulder peak is observed at about 713 nm. The disparity in excitation-emission maps in water and ethanol indicates that CDs have distinct energy gaps in various solvents.[109] A prior study found that when the polarity of the solvent was increased, the absorption wavelength of CDs redshifted.[109] In addition, colloidal CDs in the water in the quartz cuvette is observed as blue under sunlight but emit red light when excited with white light, as shown in figure 3.22f. As demonstrated in Fig. 3.22g, LLC

solution containing CDs was spin-coated onto a glass substrate and exposed to sunlight and after that and illuminated with white light. Upon white light illumination, a thin film of LLC mesophase containing CDs emits red light (see figure 3.22g). It is worth mentioning that red fluorescence emission is exhibited by both aqueous solution and LLC mesophase thin films containing CDs.

Plasmon-exciton coupling between SPPs of silver thin film and excitons of CDs was achieved by utilizing Kretschmann configuration (see figure 3.24a).[75]Among other configurations, Kretschmann configuration is mostly the preferred method for excitation of surface plasmons on metal thin films. Metal thin films are the source of surface plasmons. If surface plasmons on the metal thin films and incoming photons are in resonance, SPPs can be excited. To be able to excite SPPs on the surface of the metal thin films, photons cannot be utilized directly owing to momentum mismatch. To defeat momentum mismatch, Kretschman configuration was used. In Kretschmann configuration, a glass prism is used to enhance the momentum of the incident photon in order to achieve excitation of SPPs.

To investigate the interaction between propagating surface plasmon polaritons of flat Ag thin film and excitons of CDs at each angle of incidence, spectroscopic reflection measurements, which depend on polarization, were taken as shown in figure 3.24b. Tunable supercontinuum laser light source having a spectral width of around 1 nm was utilized to achieve surface plasmon polariton dispersion curve of bare flat Ag thin film as shown in figure 10c. Surface plasmon polariton dispersion curve of bare Ag film and dispersion curve of a 60 nm thick Ag film coated with CD was the finite time-domain (FDTD) simulated to corroborate the experimental results with theoretical results as shown in figures 3.24d, 3.24f, and 3.24h, respectively. As seen in Figure 3.24, theoretical calculations and experimental data agree with each other. The dispersion curve of bare flat Ag thin film does not possess anticrossing behavior whereas anticrossing behavior proves that there is the strong interaction between the SPPs of bare flat Ag thin film (60 nm) and excitons of CDs. While the maximum absorbance of CDs in water is around 610 nm, it is 625 nm in LLC mesophases as shown in figure 3.25.
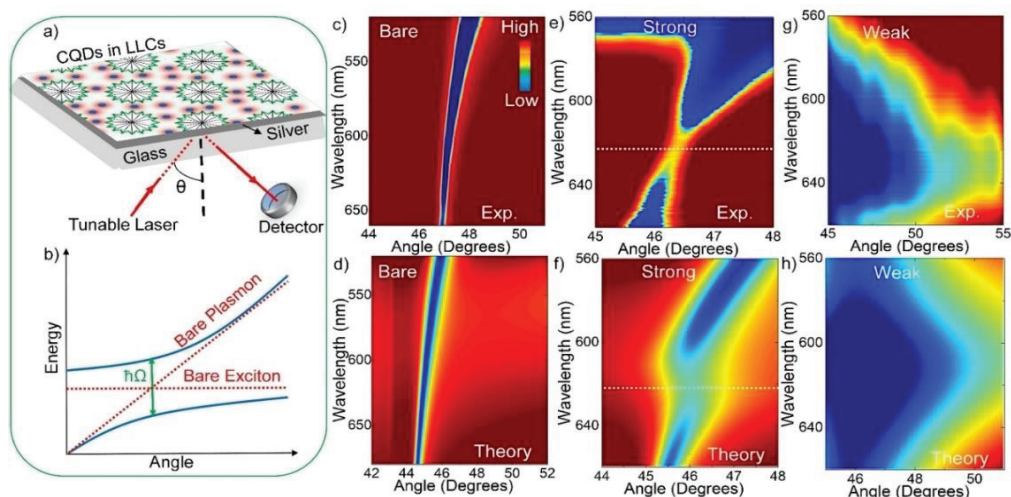
Figure 3.24. (a) The experimental setup utilized to excite surface plasmons on flat Ag thin film is depicted schematically. (b) The strong coupling observed between excitons of CDs and surface plasmon polaritons of flat Ag thin film is depicted schematically. Anticrossing occurs in the strong plasmon-exciton interaction. (c) Experimentally achieved surface plasmon polariton dispersion curve from a bare flat Ag thin film. (d) Theoretically achieved surface plasmon polariton dispersion curve from a bare silver film. (e) Experimentally achieved dispersion curve from a 60 nm thick Ag film coated with CDs. (f) Theoretically achieved polariton dispersion curve of Ag film coated with Lorentz oscillator which has the same resonance wavelength and linewidth as the CDs. High and low reflectivity are indicated sequentially by red and blue colors. At around 625 nm which is the same resonance as that of CDs in LLC solution, an anticrossing was obtained both in the experimental and theoretical dispersion curves. (g) Experimentally achieved dispersion curve from a 25 nm thick Ag film coated with CDs. (h) Theoretically achieved polariton dispersion curve of a 25 nm thick Ag film coated with Lorentz oscillator which has the same resonance wavelength and linewidth as the CDs. [13] Reprinted with permission from Sarisozen, S.; Polat, N.; Mert Balci, F.; Guvenc, C. M.; Kocabas, C.; Yaglioglu, H. G.; Balci, S. Strong Coupling of Carbon Quantum Dots in Liquid Crystals. The Journal of Physical Chemistry Letters 2022, 3562–3570. https://doi.org/10.1021/acs.jpclett.1c03937. Copyright 2022 American Chemical Society.

Indeed, anticrossing was achieved both in the experimental and theoretical dispersion curves at around 625 nm which is the same resonance as that of CDs in LLC mesophase as shown in Figures 3.24e and 3.24f. For the strong coupling to occur between SPPs of Ag thin film and excitons of CDs is $2g > |\gamma_e + \gamma_{pl}|/2$ where $2g$, γ_e, and γ_{pl} are the Rabi

splitting energy (~90 meV), the linewidth of the exciton (~75 meV), and the linewidth of the plasmon polariton (~100 meV for 60 nm thick Ag film).[110–112]
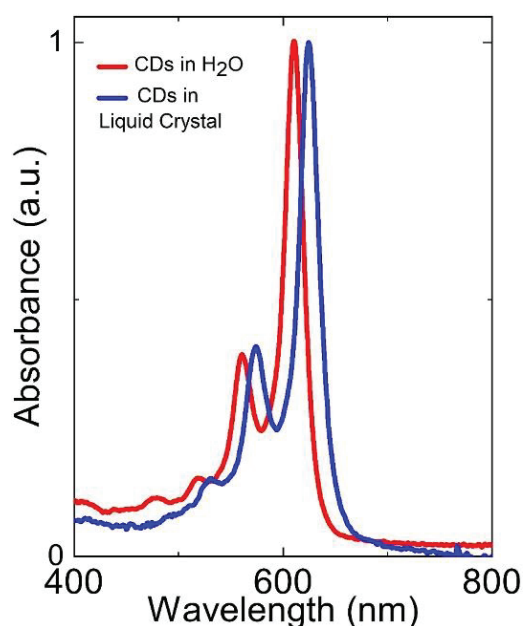
Figure 3.25. UV-vis absorbance spectra of CDs in water and in the hexagonal LLC mesophase. [13] Reprinted with permission from Sarisozen, S.; Polat, N.; Mert Balci, F.; Guvenc, C. M.; Kocabas, C.; Yaglioglu, H. G.; Balci, S. Strong Coupling of Carbon Quantum Dots in Liquid Crystals. The Journal of Physical Chemistry Letters 2022, 3562–3570. https://doi.org/10.1021/acs.jpclett.1c03937. Copyright 2022 American Chemical Society.

In fact, the theoretical calculations given in Figure 10f backed up the experimental results given in Figure 10e. Furthermore, as the number of excitons is enhanced, the Rabi splitting energy can be enhanced, because the Rabi splitting energy is proportional to the square root of the number of excitons.[98] In figure 3.24e, enhancing the gap between lower and upper polariton branches could not be achieved, because, on the one hand, a certain amount of carbon dots can be embedded in the liquid crystal mesophases, on the other hand, the excess amount of CDs aggregates. The change in the thickness of metal thin film allows the linewidth of SPPs to be adjusted.[98] The Ag thin film thickness was reduced to 25 nm (γ_{pl} ~300 meV) to demonstrate the weak coupling between excitons of CDs and surface plasmon polaritons of Ag thin film. In a prior study[98] in the literature showed that by changing the metal film thickness, the interaction between surface plasmon polaritons and excitons can be adjusted. There is no splitting at the maxima of the absorption peak

of CDs (~ 625nm) in the liquid crystal mesophase in the dispersion curves obtained both experimentally and theoretically as shown in figures 3.24g and 3.24h.

In this study, the photostability of the TDBC dye, which is the most common exciton source, and the synthesized CDs were compared in the final step as shown in figure 3.26. To do this, a continuous-wave blue laser at 488 nm and having an optical power of 50 mW was used to irradiate the aqueous solution of TDBC and synthesized CDs. The peak of the TDBC losses its appearance in the absorption spectrum which demonstrates that TDBC undergoes rapid photodegradation if it is irradiated with laser light. The CDs, in particular, are extremely stable against laser irradiation at room temperature. When J-aggregate dyes TDBC, widely employed in strong light-matter interaction experiments, and synthesized CDs were compared, the following conclusions were reached; (i) compared to TDBC, better photostability is possessed by CDs, (ii) their absorption linewidths are comparable, (iii) CDs can be synthesized in high yields and in a short time whereas difficult synthetic procedures and much more time are needed for the synthesis of J-aggregates, and (iv) CDs and J-aggregates on metal thin films with the same oscillator strength have Rabi splitting energies that are remarkably similar as demonstrated by theoretical calculations. As a result, colloidal CDs have a promising future in research involving intense light-matter interactions.
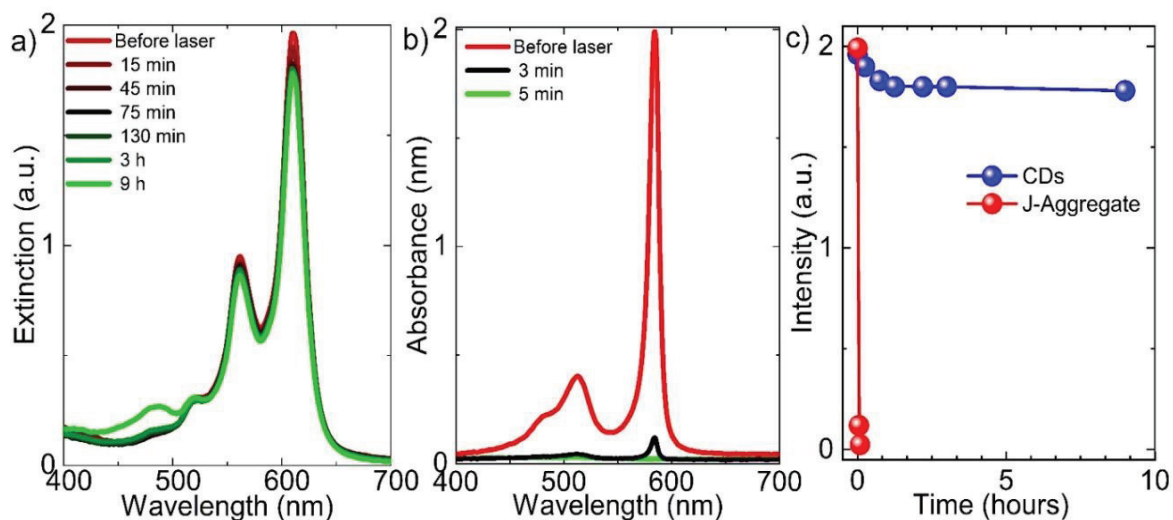
Figure 3.26. (a) Change in absorption peak intensity of CDs exposed to laser light. See that the photostability of CDs is very high when exposed to laser light at 488 nm. (b) Change in absorption peak intensity of J-aggregate dye, TDBC exposed to laser light at 488 nm. (c) Blue and red colors indicate the absorbance peak intensity of CDs and J-aggregate dye, TDBC variations as a function of time. [13] Reprinted with permission from Sarisozen, S.; Polat, N.; Mert Balci, F.; Guvenc, C. M.; Kocabas, C.; Yaglioglu, H. G.; Balci, S. Strong Coupling of Carbon Quantum Dots in Liquid Crystals. The Journal of Physical Chemistry Letters 2022, 3562–3570. https://doi.org/10.1021/acs.jpclett.1c03937. Copyright 2022 American Chemical Society.

CHAPTER 4

CONCLUSION

First, colloidal nanodisk shaped plexcitonic nanoparticles were demonstrated for the first time with extremely high Rabi splitting energies, exceeding 350 meV. Seed-mediated synthesis was utilized to obtain Ag nanoprisms, followed by shape transformation from nanoprism to nanodisk under high temperature. Ag atoms in the corners of Ag nanoprisms exposed to high temperature dissolved and then silver ions were readsorbed on the side surfaces of Ag nanoprisms, thus Ag nanodisks are generated. Under the influence of heat localized plasmon resonance frequencies of Ag nanodisks were adjusted. Then, to be able to fabricate nanodisk shaped plexcitonic nanoparticles, a cyanine dye called TDBC was utilized. TDBC self-assemble on the Ag nanodisk to yield plexcitonic nanoparticles in the aqueous environment. Localized surface plasmon polaritons of Ag nanodisks and excitons of J-aggregate, TDBC, strongly couple to create nanodisk shaped plexcitonic nanoparticles. The theoretical simulation of single plexcitonic and nanodisk shaped nanoparticles agreed well with the experimental results. Aqueous solutions of plexitonic nanodiscs can be kept for several weeks at room temperature, that is, they are stable. The large Rabi splitting energy and good stability at room temperature of plexcitonic nanoparticles expand their application areas, for example in plasmon laser, biosensor, solar cells, and molecular nanophotonics active devices.[113] For studying energy flow at nanoscale dimensions, the plexcitonic nanoparticles can be utilized to create a range of nanophotonic devices.[113,114] Furthermore, because a high yield of pure colloidal plexcitonic nanoparticles can be synthesized, large area plexcitonic devices can be produced by combining with two-dimensional nanomaterials like graphene.[115]

Secondly, laser-induced synthesis of anisotropic noble metal nanocrystals and colloidal synthesis of bimetallic decahedral shaped plexcitonic nanocrystals with adjustable optical characteristics in the visible range have both been demonstrated. Spherical Ag nanoparticles were irradiated by blue laser having 50 mW at 488 nm in order to photochemically synthesize Ag decahedral nanocrystals. Centrifugation was

utilized to separate the monocolored Ag prism shaped nanoparticles from the bicolored Ag decahedral nanoparticles after the laser aided production. Besides, the optical characteristics of decahedral nanoparticles can be altered by introducing gold ions into reaction medium. Upon addition of gold ions, galvanic displacement reaction between silver atoms and gold ions occurs. This, electrochemical reaction changes the optical properties of decahedral shaped nanoparticles. Excitons of J-aggregate dyes and SPPs of bimetallic decahedral shaped nanoparticles interact in the strong coupling regime, resulting in decahedral plexcitonic nanoparticles. Localized SPP of bimetallic decahedral shaped nanoparticles couples in the strong coupling regime with the propagating SPPs of Ag thin film, resulting in the generation of novel hybrid polaritonic modes. The electromagnetic field can be localized in a very tiny region owing to extremely sharp corners of Ag-Au bimetallic decahedral shaped nanoparticles. Gaining more insight about light–matter interaction at nanoscale levels can be done with decahedral shaped plexcitonic nanoparticles with better and controllable optical characteristics in the visible range.

Finally, weak and strong coupling of CDs in LLC mesophases are achieved for the first time by embedding hydrothermally synthesized red emissive, water-soluble CDs with high yield having an average diameter of around 4 nm into LLC mesophase and coating onto Ag thin film. Also, high crystallinity and both very sharp linewidth spectral absorbance and emission are possessed by synthesized red light-emitting CDs. The photoluminescence (red emission) of the CDs synthesized on a wide scale using a simple hydrothermal process is highly stable and strong. The fluorescence of synthesized CDs displays excitation-independent emission behavior. The Quantum yield of red emissive CDs is around 35.4 percent (in ethanol) and their lifetime is at around 2 ns in an aqueous acidic solution. Ultrafast transient absorption spectroscopy (fs-TA) was used to investigate the excited state dynamics of the produced CDs. After neutralization, CDs were dispersed in the LLC mesophases. In reality, the CDs were embedded in the hydrophilic domains of LLC mesophases. LLC solution containing CDs was spin coated onto Ag thin film. Upon spin coating, thin film with red emission was formed on top of the Ag film. Excitons of CDs and propagating surface plasmon polaritons of thin Ag films interact substantially, as evidenced by polarization-dependent spectroscopic reflection studies, and a plasmon-exciton hybrid state can be seen in the polariton dispersion curve. When J-aggregate dyes TDBC, widely employed in strong light-matter interaction experiments, and synthesized CDs were compared, the following conclusions

were reached; (i) compared to TDBC, better photostability is possessed by CDs, (ii) their absorption linewidths are comparable, (iii) CDs can be synthesized in high yields and in a short time whereas difficult synthetic procedures and much more time are needed for the synthesis of J-aggregates, and (iv) CDs and J-aggregates on metal thin films with the same oscillator strength have Rabi splitting energies that are remarkably similar as demonstrated by theoretical calculations. As a result of the unique properties and advantages of CDs such as low cost, ease of synthesis, water-solubility, bright and strong fluorescence with very narrow absorption linewidths, high quantum yields, high photostability, low toxicity, and tunable emission in the visible and near-infrared regions of the electromagnetic spectrum, CDs are witnessed the rapid increase in their usage in many applications, e.g., in optoelectronic devices, nanoscale light sources, drug delivery, bioimaging, biosensing.

REFERENCES

(1)   Amin, M. T.; Alazba, A. A.; Manzoor, U. A Review of Removal of Pollutants from Water/Wastewater Using Different Types of Nanomaterials. *Advances in Materials Science and Engineering*. 2014. https://doi.org/10.1155/2014/825910.

(2)   Xia, Y.; Xiong, Y.; Lim, B.; Skrabalak, S. E. Shape-Controlled Synthesis of Metal Nanocrystals: Simple Chemistry Meets Complex Physics? *Angewandte Chemie - International Edition*. 2009. https://doi.org/10.1002/anie.200802248.

(3)   Dreaden, E. C.; Alkilany, A. M.; Huang, X.; Murphy, C. J.; El-Sayed, M. A. The Golden Age: Gold Nanoparticles for Biomedicine. *Chemical Society Reviews* **2012**, *41* (7). https://doi.org/10.1039/c1cs15237h.

(4)   Willets, K. A.; van Duyne, R. P. Localized Surface Plasmon Resonance Spectroscopy and Sensing. *Annual Review of Physical Chemistry* **2007**, *58*. https://doi.org/10.1146/annurev.physchem.58.032806.104607.

(5)   Zhang, D.; Men, L.; Chen, Q. Microfabrication and Applications of Opto-Microfluidic Sensors. *Sensors*. 2011. https://doi.org/10.3390/s110505360.

(6)   Jeon, T.; Kim, S. J.; Yoon, J.; Byun, J.; Hong, H. R.; Lee, T. W.; Kim, J. S.; Shin, B.; Kim, S. O. Hybrid Perovskites: Effective Crystal Growth for Optoelectronic Applications. *Advanced Energy Materials*. 2017. https://doi.org/10.1002/aenm.201602596.

(7)   Würthner, F.; Kaiser, T. E.; Saha-Möller, C. R. J-Aggregates: From Serendipitous Discovery to Supramolecular Engineering of Functional Dye Materials. *Angewandte Chemie - International Edition*. 2011. https://doi.org/10.1002/anie.201002307.

(8)   Bricks, J. L.; Slominskii, Y. L.; Panas, I. D.; Demchenko, A. P. Fluorescent J-Aggregates of Cyanine Dyes: Basic Research and Applications Review. *Methods and Applications in Fluorescence*. 2018. https://doi.org/10.1088/2050-6120/aa8d0d.

(9)   Satake, A.; Kobuke, Y. Artificial Photosynthetic Systems: Assemblies of Slipped Cofacial Porphyrins and Phthalocyanines Showing Strong Electronic Coupling. *Organic and Biomolecular Chemistry* **2007**, *5* (11). https://doi.org/10.1039/b703405a.

(10)   Manuel, A. P.; Kirkey, A.; Mahdi, N.; Shankar, K. Plexcitonics-Fundamental Principles and Optoelectronic Applications. *Journal of Materials Chemistry C*. 2019. https://doi.org/10.1039/C8TC05054F.

(11)   Balci, F. M.; Sarisozen, S.; Polat, N.; Balci, S. Colloidal Nanodisk Shaped Plexcitonic Nanoparticles with Large Rabi Splitting Energies. *Journal of*

Physical Chemistry C **2019**, *123* (43).
https://doi.org/10.1021/acs.jpcc.9b08834.

(12)   Balci, F. M.; Sarisozen, S.; Polat, N.; Guvenc, C. M.; Karadeniz, U.;
Tertemiz, A.; Balci, S. Laser Assisted Synthesis of Anisotropic Metal
Nanocrystals and Strong Light-Matter Coupling in Decahedral Bimetallic
Nanocrystals. *Nanoscale Advances* **2021**, *3* (6).
https://doi.org/10.1039/d0na00829j.

(13)   Sarisozen, S.; Polat, N.; Mert Balci, F.; Guvenc, C. M.; Kocabas, C.;
Yaglioglu, H. G.; Balci, S. Strong Coupling of Carbon Quantum Dots in
Liquid Crystals. *The Journal of Physical Chemistry Letters* **2022**, 3562–
3570. https://doi.org/10.1021/acs.jpclett.1c03937.

(14)   Feynman, R. Conclusion : " Plenty of Room at the Bottom ." In *Engineering
and Science*; 1959; Vol. 23 (5).

(15)   Jeevanandam, J.; Barhoum, A.; Chan, Y. S.; Dufresne, A.; Danquah, M. K.
Review on Nanoparticles and Nanostructured Materials: History, Sources,
Toxicity and Regulations. *Beilstein Journal of Nanotechnology*. 2018.
https://doi.org/10.3762/bjnano.9.98.

(16)   Ahmadi, T. S.; Wang, Z. L.; Green, T. C.; Henglein, A.; El-Sayed, M. A.
Shape-Controlled Synthesis of Colloidal Platinum Nanoparticles. *Science
(1979)* **1996**, *272* (5270). https://doi.org/10.1126/science.272.5270.1924.

(17)   Senthil Kumar, P.; Pastoriza-Santos, I.; Rodríguez-González, B.; Javier
García De Abajo, F.; Liz-Marzán, L. M. High-Yield Synthesis and Optical
Response of Gold Nanostars. *Nanotechnology* **2008**, *19* (1).
https://doi.org/10.1088/0957-4484/19/01/015606.

(18)   Sarisozen, S.; Tertemiz, N. A.; Arica, T. A.; Polat, N.; Kocabas, C.; Balci,
F. M.; Balci, S. Transition Metal Salt Promoted, Green, and High-Yield
Synthesis of Silver Nanowires for Flexible Transparent Conductive
Electrodes. *ChemistrySelect* **2021**, *6* (44).
https://doi.org/10.1002/slct.202103434.

(19)   Ramyadevi, J.; Jeyasubramanian, K.; Marikani, A.; Rajakumar, G.;
Rahuman, A. A. Synthesis and Antimicrobial Activity of Copper
Nanoparticles. *Materials Letters* **2012**, *71*.
https://doi.org/10.1016/j.matlet.2011.12.055.

(20)   Guvenc, C. M.; Balci, F. M.; Sarisozen, S.; Polat, N.; Balci, S. Colloidal
Bimetallic Nanorings for Strong Plasmon Exciton Coupling. *Journal of
Physical Chemistry C* **2020**, *124* (15).
https://doi.org/10.1021/acs.jpcc.0c01011.

(21)   Kroto, H. W.; Heath, J. R.; O'Brien, S. C.; Curl, R. F.; Smalley, R. E. C60:
Buckminsterfullerene. *Nature* **1985**, *318* (6042).
https://doi.org/10.1038/318162a0.

(22)   Iijima, S.; Ichihashi, T. Single-Shell Carbon Nanotubes of 1-Nm Diameter. *Nature* **1993**, *363* (6430). https://doi.org/10.1038/363603a0.

(23)   Protesescu, L.; Yakunin, S.; Bodnarchuk, M. I.; Krieg, F.; Caputo, R.; Hendon, C. H.; Yang, R. X.; Walsh, A.; Kovalenko, M. v. Nanocrystals of Cesium Lead Halide Perovskites (CsPbX3, X = Cl, Br, and I): Novel Optoelectronic Materials Showing Bright Emission with Wide Color Gamut. *Nano Letters* **2015**, *15* (6). https://doi.org/10.1021/nl5048779.

(24)   Peng, X.; Manna, L.; Yang, W.; Wickham, J.; Scher, E.; Kadavanich, A.; Alivisatos, A. P. Shape Control of CdSe Nanocrystals. *Nature* **2000**, *404* (6773). https://doi.org/10.1038/35003535.

(25)   Guvenc, C. M.; Yalcinkaya, Y.; Ozen, S.; Sahin, H.; Demir, M. M. Gd3+-Doped α-CsPbI3 Nanocrystals with Better Phase Stability and Optical Properties. *Journal of Physical Chemistry C* **2019**, *123* (40). https://doi.org/10.1021/acs.jpcc.9b05969.

(26)   Guvenc, C. M.; Balci, S. Seed-Mediated Synthesis of Colloidal 2D Halide Perovskite Nanoplatelets. *ChemNanoMat* **2021**, *7* (11). https://doi.org/10.1002/cnma.202100315.

(27)   Sajti, C. L.; Sattari, R.; Chichkov, B. N.; Barcikowski, S. Gram Scale Synthesis of Pure Ceramic Nanoparticles by Laser Ablation in Liquid. *Journal of Physical Chemistry C* **2010**, *114* (6). https://doi.org/10.1021/jp906960g.

(28)   Sigmund, W.; Yuh, J.; Park, H.; Maneeratana, V.; Pyrgiotakis, G.; Daga, A.; Taylor, J.; Nino, J. C. Processing and Structure Relationships in Electrospinning of Ceramic Fiber Systems. *Journal of the American Ceramic Society* **2006**, *89* (2). https://doi.org/10.1111/j.1551-2916.2005.00807.x.

(29)   Rao, J. P.; Geckeler, K. E. Polymer Nanoparticles: Preparation Techniques and Size-Control Parameters. *Progress in Polymer Science (Oxford)*. 2011. https://doi.org/10.1016/j.progpolymsci.2011.01.001.

(30)   Puri, A.; Loomis, K.; Smith, B.; Lee, J. H.; Yavlovich, A.; Heldman, E.; Blumenthal, R. Lipid-Based Nanoparticles as Pharmaceutical Drug Carriers: From Concepts to Clinic. *Critical Reviews in Therapeutic Drug Carrier Systems*. 2009. https://doi.org/10.1615/CritRevTherDrugCarrierSyst.v26.i6.10.

(31)   Faraday, M. Experimental Relations o f Gold (and Other Metals) to Light. *Phil. Trans. R. Soc.* **1857**, *147* (0).

(32)   Balci, S. Ultrastrong Plasmon–Exciton Coupling in Metal Nanoprisms with J-Aggregates. *Optics Letters* **2013**, *38* (21). https://doi.org/10.1364/ol.38.004498.

(33)   Pérez-Juste, J.; Pastoriza-Santos, I.; Liz-Marzán, L. M.; Mulvaney, P. Gold Nanorods: Synthesis, Characterization and Applications. In *Coordination*

Chemistry Reviews; 2005; Vol. 249.
https://doi.org/10.1016/j.ccr.2005.01.030.

(34)   Skrabalak, S. E.; Au, L.; Li, X.; Xia, Y. Facile Synthesis of Ag Nanocubes
         and Au Nanocages. *Nature Protocols* **2007**, *2* (9).
         https://doi.org/10.1038/nprot.2007.326.

(35)   Yavuz, M. S.; Cheng, Y.; Chen, J.; Cobley, C. M.; Zhang, Q.; Rycenga, M.;
         Xie, J.; Kim, C.; Song, K. H.; Schwartz, A. G.; Wang, L. v.; Xia, Y. Gold
         Nanocages Covered by Smart Polymers for Controlled Release with Near-
         Infrared Light. *Nature Materials* **2009**, *8* (12).
         https://doi.org/10.1038/nmat2564.

(36)   Hao, F.; Nehl, C. L.; Hafner, J. H.; Nordlander, P. Plasmon Resonances of a
         Gold Nanostar. *Nano Letters* **2007**, *7* (3). https://doi.org/10.1021/nl062969c.

(37)   Sun, Y.; Xia, Y. Large-Scale Synthesis of Uniform Silver Nanowires
         through a Soft, Self-Seeding, Polyol Process. *Advanced Materials* **2002**, *14*
         (11). https://doi.org/10.1002/1521-4095(20020605)14:11<833::AID-
         ADMA833>3.0.CO;2-K.

(38)   Ozbay, E. Plasmonics: Merging Photonics and Electronics at Nanoscale
         Dimensions. *Science*. 2006. https://doi.org/10.1126/science.1114849.

(39)   Barnes, W. L.; Dereux, A.; Ebbesen, T. W. Surface Plasmon Subwavelength
         Optics. *Nature*. 2003. https://doi.org/10.1038/nature01937.

(40)   Yuen-Zhou, J.; Saikin, S. K.; Zhu, T.; Onbasli, M. C.; Ross, C. A.; Bulovic,
         V.; Baldo, M. A. Plexciton Dirac Points and Topological Modes. *Nature
         Communications* **2016**, *7*. https://doi.org/10.1038/ncomms11783.

(41)   Xu, X.; Ray, R.; Gu, Y.; Ploehn, H. J.; Gearheart, L.; Raker, K.; Scrivens,
         W. A. Electrophoretic Analysis and Purification of Fluorescent Single-
         Walled Carbon Nanotube Fragments. *J Am Chem Soc* **2004**, *126* (40).
         https://doi.org/10.1021/ja040082h.

(42)   Feng, X.; Jiang, Y.; Zhao, J.; Miao, M.; Cao, S.; Fang, J.; Shi, L. Easy
         Synthesis of Photoluminescent N-Doped Carbon Dots from Winter Melon
         for Bio-Imaging. *RSC Advances* **2015**, *5* (40).
         https://doi.org/10.1039/c5ra02271a.

(43)   de Medeiros, T. v.; Manioudakis, J.; Noun, F.; Macairan, J. R.; Victoria, F.;
         Naccache, R. Microwave-Assisted Synthesis of Carbon Dots and Their
         Applications. *Journal of Materials Chemistry C* **2019**, *7* (24).
         https://doi.org/10.1039/c9tc01640f.

(44)   Sun, Y. P.; Zhou, B.; Lin, Y.; Wang, W.; Fernando, K. A. S.; Pathak, P.;
         Meziani, M. J.; Harruff, B. A.; Wang, X.; Wang, H.; Luo, P. G.; Yang, H.;
         Kose, M. E.; Chen, B.; Veca, L. M.; Xie, S. Y. Quantum-Sized Carbon Dots
         for Bright and Colorful Photoluminescence. *J Am Chem Soc* **2006**, *128* (24).
         https://doi.org/10.1021/ja062677d.

(45) Zhou, J.; Booker, C.; Li, R.; Zhou, X.; Sham, T. K.; Sun, X.; Ding, Z. An Electrochemical Avenue to Blue Luminescent Nanocrystals from Multiwalled Carbon Nanotubes (MWCNTs). *J Am Chem Soc* **2007**, *129* (4). https://doi.org/10.1021/ja0669070.

(46) Zhu, S.; Song, Y.; Wang, J.; Wan, H.; Zhang, Y.; Ning, Y.; Yang, B. Photoluminescence Mechanism in Graphene Quantum Dots: Quantum Confinement Effect and Surface/Edge State. *Nano Today* **2017**, *13*. https://doi.org/10.1016/j.nantod.2016.12.006.

(47) Couto, O. D. D.; Puebla, J.; Chekhovich, E. A.; Luxmoore, I. J.; Elliott, C. J.; Babazadeh, N.; Skolnick, M. S.; Tartakovskii, A. I.; Krysa, A. B. Charge Control in InP/(Ga,In)P Single Quantum Dots Embedded in Schottky Diodes. *Physical Review B - Condensed Matter and Materials Physics* **2011**, *84* (12). https://doi.org/10.1103/PhysRevB.84.125301.

(48) Yuan, F.; Yuan, T.; Sui, L.; Wang, Z.; Xi, Z.; Li, Y.; Li, X.; Fan, L.; Tan, Z.; Chen, A.; Jin, M.; Yang, S. Engineering Triangular Carbon Quantum Dots with Unprecedented Narrow Bandwidth Emission for Multicolored LEDs. *Nature Communications* **2018**, *9* (1). https://doi.org/10.1038/s41467-018-04635-5.

(49) Yue, L.; Li, H.; Sun, Q.; Zhang, J.; Luo, X.; Wu, F.; Zhu, X. Red-Emissive Ruthenium-Containing Carbon Dots for Bioimaging and Photodynamic Cancer Therapy. *ACS Applied Nano Materials* **2020**, *3* (1). https://doi.org/10.1021/acsanm.9b02394.

(50) Peng, Z.; Han, X.; Li, S.; Al-Youbi, A. O.; Bashammakh, A. S.; El-Shahawi, M. S.; Leblanc, R. M. Carbon Dots: Biomacromolecule Interaction, Bioimaging and Nanomedicine. *Coordination Chemistry Reviews*. 2017. https://doi.org/10.1016/j.ccr.2017.06.001.

(51) Ritchie, R. H. Plasma Losses by Fast Electrons in Thin Films. *Physical Review* **1957**, *106* (5). https://doi.org/10.1103/PhysRev.106.874.

(52) Pala, R. A.; White, J.; Barnard, E.; Liu, J.; Brongersma, M. L. Design of Plasmonic Thin-Film Solar Cells with Broadband Absorption Enhancements. *Advanced Materials* **2009**, *21* (34). https://doi.org/10.1002/adma.200900331.

(53) Odom, T. W.; Schatz, G. C. Introduction to Plasmonics. *Chemical Reviews*. 2011. https://doi.org/10.1021/cr2001349.

(54) Guedje, F. K.; Giloan, M.; Potara, M.; Hounkonnou, M. N.; Astilean, S. Optical Properties of Single Silver Triangular Nanoprism. *Physica Scripta* **2012**, *86* (5). https://doi.org/10.1088/0031-8949/86/05/055702.

(55) Aslan, K.; Wu, M.; Lakowicz, J. R.; Geddes, C. D. Fluorescent Core-Shell Ag@SiO2 Nanocomposites for Metal-Enhanced Fluorescence and Single Nanoparticle Sensing Platforms. *J Am Chem Soc* **2007**, *129* (6). https://doi.org/10.1021/ja0680820.

(56)   Leong, H. S.; Guo, J.; Lindquist, R. G.; Liu, Q. H. Surface Plasmon Resonance in Nanostructured Metal Films under the Kretschmann Configuration. *Journal of Applied Physics* **2009**, *106* (12). https://doi.org/10.1063/1.3273359.

(57)   Akowuah, E. K.; Gorman, T.; Haxha, S. Design and Optimization of a Novel Surface Plasmon Resonance Biosensor Based on Otto Configuration. *Optics Express* **2009**, *17* (26). https://doi.org/10.1364/oe.17.023511.

(58)   Yeh, W. H.; Kleingartner, J.; Hillier, A. C. Wavelength Tunable Surface Plasmon Resonance-Enhanced Optical Transmission through a Chirped Diffraction Grating. *Analytical Chemistry* **2010**, *82* (12). https://doi.org/10.1021/ac100497w.

(59)   Pockrand, I.; Brillante, A.; Möbius, D. Exciton-Surface Plasmon Coupling: An Experimental Investigation. *The Journal of Chemical Physics* **1982**, *77*. https://doi.org/10.1063/1.443834.

(60)   Couto, O. D. D.; Puebla, J.; Chekhovich, E. A.; Luxmoore, I. J.; Elliott, C. J.; Babazadeh, N.; Skolnick, M. S.; Tartakovskii, A. I.; Krysa, A. B. Charge Control in InP/(Ga,In)P Single Quantum Dots Embedded in Schottky Diodes. *Physical Review B - Condensed Matter and Materials Physics* **2011**, *84* (12). https://doi.org/10.1103/PhysRevB.84.125301.

(61)   Frenkel, J. On the Transformation of Light into Heat in Solids. i. *Physical Review* **1931**, *37* (1). https://doi.org/10.1103/PhysRev.37.17.

(62)   Liang, W. Y. Excitons. *Physics Education* **1970**, *5* (4). https://doi.org/10.1088/0031-9120/5/4/003.

(63)   Kéna-Cohen, S.; Forrest, S. R. Room-Temperature Polariton Lasing in an Organic Single-Crystal Microcavity. *Nature Photonics* **2010**, *4* (6). https://doi.org/10.1038/nphoton.2010.86.

(64)   Wannier, G. H. The Structure of Electronic Excitation Levels in Insulating Crystals. *Physical Review* **1937**, *52* (3). https://doi.org/10.1103/PhysRev.52.191.

(65)   Guvenc, C. M.; Polat, N.; Balci, S. Strong Plasmon-Exciton Coupling in Colloidal Halide Perovskite Nanocrystals near a Metal Film. *Journal of Materials Chemistry C* **2020**, *8* (46). https://doi.org/10.1039/d0tc04209a.

(66)   Gómez, D. E.; Vernon, K. C.; Mulvaney, P.; Davis, T. J. Surface Plasmon Mediated Strong Exciton-Photon Coupling in Semiconductor Nanocrystals. *Nano Letters* **2010**, *10* (1). https://doi.org/10.1021/nl903455z.

(67)   Winkler, J. M.; Rabouw, F. T.; Rossinelli, A. A.; Jayanti, S. v.; McPeak, K. M.; Kim, D. K.; le Feber, B.; Prins, F.; Norris, D. J. Room-Temperature Strong Coupling of CdSe Nanoplatelets and Plasmonic Hole Arrays. *Nano Letters* **2019**, *19* (1). https://doi.org/10.1021/acs.nanolett.8b03422.

(68) Scheibe, G. Über Die Veränderlichkeit Der Absorptionsspektren in Lösungen Und Die Nebenvalenzen Als Ihre Ursache. *Angewandte Chemie* **1937**, *50* (11). https://doi.org/10.1002/ange.19370501103.

(69) Jelley, E. E. Spectral Absorption and Fluorescence of Dyes in the Molecular State [1]. *Nature*. 1936. https://doi.org/10.1038/1381009a0.

(70) von Berlepsch, H.; Böttcher, C.; Quart, A.; Burger, C.; Dähne, S.; Kirstein, S. Supramolecular Structures of J-Aggregates of Carbocyanine Dyes in Solution. *Journal of Physical Chemistry B* **2000**, *104* (22). https://doi.org/10.1021/jp000220z.

(71) Möbius, D. Scheibe Aggregates. *Advanced Materials* **1995**, *7* (5). https://doi.org/10.1002/adma.19950070503.

(72) Kirstein, S.; Möhwald, H. Exciton Band Structures in 2D Aggregates of Cyanine Dyes. *Advanced Materials* **1995**, *7* (5). https://doi.org/10.1002/adma.19950070509.

(73) Kundu, S.; Patra, A. Nanoscale Strategies for Light Harvesting. *Chemical Reviews*. 2017. https://doi.org/10.1021/acs.chemrev.6b00036.

(74) Fofang, N. T.; Park, T. H.; Neumann, O.; Mirin, N. A.; Nordlander, P.; Halas, N. J. Plexcitonic Nanoparticles: Plasmon-Exciton Coupling in Nanoshell-J- Aggregate Complexes. *Nano Letters* **2008**, *8* (10). https://doi.org/10.1021/nl8024278.

(75) Finkelstein-Shapiro, D.; Mante, P. A.; Sarisozen, S.; Wittenbecher, L.; Minda, I.; Balci, S.; Pullerits, T.; Zigmantas, D. Understanding Radiative Transitions and Relaxation Pathways in Plexcitons. *Chem* **2021**, *7* (4). https://doi.org/10.1016/j.chempr.2021.02.028.

(76) Baranov, D. G.; Wersäll, M.; Cuadra, J.; Antosiewicz, T. J.; Shegai, T. Novel Nanostructures and Materials for Strong Light-Matter Interactions. *ACS Photonics*. 2018. https://doi.org/10.1021/acsphotonics.7b00674.

(77) Reinitzer, F. Beiträge Zur Kenntniss Des Cholesterins. *Monatshefte für Chemie* **1888**, *9* (1). https://doi.org/10.1007/BF01516710.

(78) Lehmann, O. Über Fliessende Krystalle. *Zeitschrift für Physikalische Chemie* **1889**, *4U* (1). https://doi.org/10.1515/zpch-1889-0434.

(79) Vertogen, G.; de Jeu, W. H. *Thermotropic Liquid Crystals, Fundamentals*; 1988; Vol. 45.

(80) Balci, F. M.; Balci, S.; Kocabas, C.; Dag, Ö. Lyotropic Liquid-Crystalline Mesophase of Lithium Triflate-Nonionic Surfactant as Gel Electrolyte for Graphene Optical Modulator. *Journal of Physical Chemistry C* **2017**, *121* (21). https://doi.org/10.1021/acs.jpcc.7b03622.

(81) Yilmaz, E.; Olutaş, E. B.; Barim, G.; Bandara, J.; Dag, Ö. Lithium Salt-Nonionic Surfactant Lyotropic Liquid Crystalline Gel-Electrolytes with

Redox Couple for Dye Sensitized Solar Cells. *RSC Advances* **2016**, *6* (99). https://doi.org/10.1039/c6ra19979h.

(82)   Olutaş, E. B.; Balcl, F. M.; Dag, Ö. Strong Acid-Nonionic Surfactant Lyotropic Liquid-Crystalline Mesophases as Media for the Synthesis of Carbon Quantum Dots and Highly Proton Conducting Mesostructured Silica Thin Films and Monoliths. *Langmuir* **2015**, *31* (37). https://doi.org/10.1021/acs.langmuir.5b02225.

(83)   Rajabalaya, R.; Musa, M. N.; Kifli, N.; David, S. R. Oral and Transdermal Drug Delivery Systems: Role of Lipid-Based Lyotropic Liquid Crystals. *Drug Design, Development and Therapy*. 2017. https://doi.org/10.2147/DDDT.S103505.

(84)   Balci, S. Ultrastrong Plasmon–Exciton Coupling in Metal Nanoprisms with J-Aggregates. *Optics Letters* **2013**, *38* (21). https://doi.org/10.1364/ol.38.004498.

(85)   Balci, S.; Kucukoz, B.; Balci, O.; Karatay, A.; Kocabas, C.; Yaglioglu, G. Tunable Plexcitonic Nanoparticles: A Model System for Studying Plasmon-Exciton Interaction from the Weak to the Ultrastrong Coupling Regime. *ACS Photonics* **2016**, *3* (11). https://doi.org/10.1021/acsphotonics.6b00498.

(86)   Tang, B.; Xu, S.; Hou, X.; Li, J.; Sun, L.; Xu, W.; Wang, X. Shape Evolution of Silver Nanoplates through Heating and Photoinduction. *ACS Applied Materials and Interfaces* **2013**, *5* (3). https://doi.org/10.1021/am302072u.

(87)   Pietrobon, B.; Kitaev, V. Photochemical Synthesis of Monodisperse Size-Controlled Silver Decahedral Nanoparticles and Their Remarkable Optical Properties. *Chemistry of Materials* **2008**, *20* (16). https://doi.org/10.1021/cm800926u.

(88)   Balci, S.; Karademir, E.; Kocabas, C. Strong Coupling between Localized and Propagating Plasmon Polaritons. *Optics Letters* **2015**, *40* (13). https://doi.org/10.1364/ol.40.003177.

(89)   Kelly, K. L.; Coronado, E.; Zhao, L. L.; Schatz, G. C. The Optical Properties of Metal Nanoparticles: The Influence of Size, Shape, and Dielectric Environment. *Journal of Physical Chemistry B* **2003**, *107* (3). https://doi.org/10.1021/jp026731y.

(90)   Jin, R.; Cao, Y. C.; Hao, E.; Métraux, G. S.; Schatz, G. C.; Mirkin, C. A. Controlling Anisotropic Nanoparticle Growth through Plasmon Excitation. *Nature* **2003**, *425* (6957). https://doi.org/10.1038/nature02020.

(91)   Jin, R.; Cao, Y.; Mirkin, C. A.; Kelly, K. L.; Schatz, G. C.; Zheng, J. G. Photoinduced Conversion of Silver Nanospheres to Nanoprisms. *Science (1979)* **2001**, *294* (5548). https://doi.org/10.1126/science.1066541.

(92)   Tang, B.; An, J.; Zheng, X.; Xu, S.; Li, D.; Zhou, J.; Zhao, B.; Xu, W. Silver Nanodisks with Tunable Size by Heat Aging. *Journal of Physical Chemistry C* **2008**, *112* (47). https://doi.org/10.1021/jp806486f.

(93)   Chen, S.; Fan, Z.; Carroll, D. L. Silver Nanodisks: Synthesis, Characterization, and Self-Assembly. *Journal of Physical Chemistry B*. 2002. https://doi.org/10.1021/jp026376b.

(94)   Zhang, Q.; Ge, J.; Pham, T.; Goebl, J.; Hu, Y.; Lu, Z.; Yin, Y. Reconstruction of Silver Nanoplates by UV Irradiation: Tailored Optical Properties and Enhanced Stability. *Angewandte Chemie - International Edition* **2009**, *48* (19). https://doi.org/10.1002/anie.200900545.

(95)   Liu, L.; Burnyeat, C. A.; Lepsenyi, R. S.; Nwabuko, I. O.; Kelly, T. L. Mechanism of Shape Evolution in Ag Nanoprisms Stabilized by Thiol-Terminated Poly(Ethylene Glycol): An in Situ Kinetic Study. *Chemistry of Materials* **2013**, *25* (21). https://doi.org/10.1021/cm401944b.

(96)   Tischler, J. R.; Scott Bradley, M.; Zhang, Q.; Atay, T.; Nurmikko, A.; Bulović, V. Solid State Cavity QED: Strong Coupling in Organic Thin Films. *Organic Electronics* **2007**, *8* (2–3). https://doi.org/10.1016/j.orgel.2007.01.008.

(97)   Vasa, P.; Lienau, C. Strong Light-Matter Interaction in Quantum Emitter/Metal Hybrid Nanostructures. *ACS Photonics*. 2018. https://doi.org/10.1021/acsphotonics.7b00650.

(98)   Balci, S.; Kocabas, C.; Ates, S.; Karademir, E.; Salihoglu, O.; Aydinli, A. Tuning Surface Plasmon-Exciton Coupling via Thickness Dependent Plasmon Damping. *Physical Review B - Condensed Matter and Materials Physics* **2012**, *86* (23). https://doi.org/10.1103/PhysRevB.86.235402.

(99)   Kuladeep, R.; Jyothi, L.; Alee, K. S.; Deepak, K. L. N.; Rao, D. N. Laser-Assisted Synthesis of Au-Ag Alloy Nanoparticles with Tunable Surface Plasmon Resonance Frequency. *Optical Materials Express* **2012**, *2* (2). https://doi.org/10.1364/ome.2.000161.

(100)   Peng, Z.; Spliethoff, B.; Tesche, B.; Walther, T.; Kleinermanns, K. Laser-Assisted Synthesis of Au - Ag Alloy Nanoparticles in Solution. *Journal of Physical Chemistry B* **2006**, *110* (6). https://doi.org/10.1021/jp056677w.

(101)   Chikkaraddy, R.; de Nijs, B.; Benz, F.; Barrow, S. J.; Scherman, O. A.; Rosta, E.; Demetriadou, A.; Fox, P.; Hess, O.; Baumberg, J. J. Single-Molecule Strong Coupling at Room Temperature in Plasmonic Nanocavities. *Nature* **2016**, *535* (7610). https://doi.org/10.1038/nature17974.

(102)   Moreau, A.; Ciracì, C.; Mock, J. J.; Smith, D. R.; Hill, R. T.; Chilkoti, A.; Wang, Q.; Wiley, B. J. Controlled-Reflectance Surfaces with Film-Coupled Colloidal Nanoantennas. *Nature*. 2012. https://doi.org/10.1038/nature11615.

(103) Mock, J. J.; Hill, R. T.; Degiron, A.; Zauscher, S.; Chilkoti, A.; Smith, D. R. Distance-Dependent Plasmon Resonant Coupling between a Gold Nanoparticle and Gold Film. *Nano Letters* **2008**, *8* (8). https://doi.org/10.1021/nl080872f.

(104) Lin, C. C.; Lee, L. T.; Hsu, L. J. Degradation of Polyvinyl Alcohol in Aqueous Solutions Using UV-365 Nm/S2O82- Process. *International Journal of Environmental Science and Technology* **2014**, *11* (3). https://doi.org/10.1007/s13762-013-0280-6.

(105) Dong, Y.; Pang, H.; Yang, H. bin; Guo, C.; Shao, J.; Chi, Y.; Li, C. M.; Yu, T. Carbon-Based Dots Co-Doped with Nitrogen and Sulfur for High Quantum Yield and Excitation-Independent Emission. *Angewandte Chemie - International Edition* **2013**, *52* (30). https://doi.org/10.1002/anie.201301114.

(106) Gong, J.; Lu, X.; An, X. Carbon Dots as Fluorescent Off-on Nanosensors for Ascorbic Acid Detection. *RSC Advances* **2015**, *5* (11). https://doi.org/10.1039/c4ra13576h.

(107) Liu, J.; Geng, Y.; Li, D.; Yao, H.; Huo, Z.; Li, Y.; Zhang, K.; Zhu, S.; Wei, H.; Xu, W.; Jiang, J.; Yang, B. Deep Red Emissive Carbonized Polymer Dots with Unprecedented Narrow Full Width at Half Maximum. *Advanced Materials* **2020**, *32* (17). https://doi.org/10.1002/adma.201906641.

(108) Chen, Y.; Zheng, M.; Xiao, Y.; Dong, H.; Zhang, H.; Zhuang, J.; Hu, H.; Lei, B.; Liu, Y. A Self-Quenching-Resistant Carbon-Dot Powder with Tunable Solid-State Fluorescence and Construction of Dual-Fluorescence Morphologies for White Light-Emission. *Advanced Materials* **2016**, *28* (2). https://doi.org/10.1002/adma.201503380.

(109) Wang, H.; Sun, C.; Chen, X.; Zhang, Y.; Colvin, V. L.; Rice, Q.; Seo, J.; Feng, S.; Wang, S.; Yu, W. W. Excitation Wavelength Independent Visible Color Emission of Carbon Dots. *Nanoscale* **2017**, *9* (5). https://doi.org/10.1039/c6nr09200d.

(110) Khitrova, G.; Gibbs, H. M.; Kira, M.; Koch, S. W.; Scherer, A. Vacuum Rabi Splitting in Semiconductors. *Nature Physics*. 2006. https://doi.org/10.1038/nphys227.

(111) Carlson, C.; Salzwedel, R.; Selig, M.; Knorr, A.; Hughes, S. Strong Coupling Regime and Hybrid Quasinormal Modes from a Single Plasmonic Resonator Coupled to a Transition Metal Dichalcogenide Monolayer. *Physical Review B* **2021**, *104* (12). https://doi.org/10.1103/PhysRevB.104.125424.

(112) Zengin, G.; Wersäll, M.; Nilsson, S.; Antosiewicz, T. J.; Käll, M.; Shegai, T. Realizing Strong Light-Matter Interactions between Single-Nanoparticle Plasmons and Molecular Excitons at Ambient Conditions. *Physical Review Letters* **2015**, *114* (15). https://doi.org/10.1103/PhysRevLett.114.157401.

(113) Yuen-Zhou, J.; Saikin, S. K.; Zhu, T.; Onbasli, M. C.; Ross, C. A.; Bulovic, V.; Baldo, M. A. Plexciton Dirac Points and Topological Modes. *Nature Communications* **2016**, *7*. https://doi.org/10.1038/ncomms11783.

(114) Zakharko, Y.; Rother, M.; Graf, A.; Hähnlein, B.; Brohmann, M.; Pezoldt, J.; Zaumseil, J. Radiative Pumping and Propagation of Plexcitons in Diffractive Plasmonic Crystals. *Nano Letters* **2018**, *18* (8). https://doi.org/10.1021/acs.nanolett.8b01733.

(115) Balci, S.; Balci, O.; Kakenov, N.; Atar, F. B.; Kocabas, C. Dynamic Tuning of Plasmon Resonance in the Visible Using Graphene. *Optics Letters* **2016**, *41* (6). https://doi.org/10.1364/ol.41.001241.